

CIRCUMSTELLAR DUST AROUND AGB STARS AND IMPLICATIONS FOR INFRARED EMISSION FROM GALAXIES

ALEXA VILLAUME¹, CHARLIE CONROY², AND BENJAMIN D. JOHNSON²

Draft version October 1, 2018

ABSTRACT

Stellar population synthesis (SPS) models are used to infer many galactic properties including star formation histories, metallicities, and stellar and dust masses. However, most SPS models neglect the effect of circumstellar dust shells around evolved stars and it is unclear to what extent they impact the analysis of SEDs. To overcome this shortcoming we have created a new set of circumstellar dust models, using the radiative transfer code DUSTY (Ivezic et al. 1999), for asymptotic giant branch (AGB) stars and incorporated them into the Flexible Stellar Population Synthesis code. The circumstellar dust models provide a good fit to individual AGB stars as well as the IR color-magnitude diagrams of the Large and Small Magellanic Clouds. IR luminosity functions from the Large and Small Magellanic Clouds are not well-fit by the 2008 Padova isochrones when coupled to our circumstellar dust models, and so we adjusted the lifetimes of AGB stars in the models to provide a match to the data. We show, in agreement with previous work, that circumstellar dust from AGB stars can make a significant contribution to the IR ($\gtrsim 4\mu\text{m}$) emission from galaxies that contain relatively little diffuse dust, including low-metallicity and/or non-star forming galaxies. Our models provide a good fit to the mid-IR spectra of early-type galaxies. Circumstellar dust around AGB stars appears to have a small effect on the IR SEDs of metal-rich star-forming galaxies (i.e., when $A_V \gtrsim 0.1$). Stellar population models that include circumstellar dust will be needed to accurately interpret data from the James Webb Space Telescope (JWST) and other IR facilities.

Subject headings: stars: AGB and post-AGB – infrared: galaxies — galaxies: stellar content

1. INTRODUCTION

The physical structure, past history, and current properties of a galaxy all go into shaping its observed spectral energy distribution (SED). As such, SEDs are powerful sources of information for unresolved galaxies and have long been used to discern the underlying physical properties of galaxies beginning with the work of Tinsley (1972), Searle et al. (1973), and Larson & Tinsley (1978). These studies pioneered the method of creating synthetic galactic spectra through the sum of the spectra of the stars hosted by the galaxy that has since become known as stellar population synthesis (SPS). By fitting galaxy SEDs with SPS models, properties of the galaxy such as the star formation rate, total mass in stars, metallicity, dust content, and the star formation history can be estimated. For details on the inner workings of SPS models and their broader impact we refer the reader to the recent reviews by Walcher et al. (2011) and Conroy (2013).

While there are exciting possibilities for the information we are able to obtain through SPS model fitting, as Charles Babbage noted when first introducing the mechanical computer, we can only expect the right answers if we provide the right input (or, colloquially, “Garbage in, Garbage Out”; Babbage 1864). The limitations of inputs to SPS models are well-known, far ranging, and much discussed. Such limitations include incomplete isochrone tables and stellar libraries, poorly understood stellar evolution, and uncertainties in the initial mass function (IMF). In this paper, we focus on circumstellar

dust around asymptotic giant branch (AGB) stars, and the extent to which it affects the integrated light of stellar populations.

The AGB phase is the last phase of stellar evolution in intermediate to low mass stars ($\sim 0.1 - 8M_\odot$) in which significant nuclear burning takes place. During this phase stars eject their envelopes (with mass loss rates up to $10^{-4}M_\odot \text{ yr}^{-1}$) and evolve toward the white dwarf cooling sequence. The material around the star is observed to be dust rich (Bedijn 1987). This phase is notoriously difficult to model owing to the difficulty in modeling (in 1D) stellar mass loss, convection, and mixing processes in the stellar interior. AGB stars are very luminous and can contribute many tens of percent to the integrated light of stellar populations (Melbourne & Boyer 2013; Conroy 2013; Melbourne et al. 2012; Kelson & Holden 2010).

The helium-shell flashes that occur during the AGB phase trigger the third dredge-up (TDU) process that brings material from the interior of the star to the surface. The surfaces of AGB stars begin as oxygen-rich ($\text{C/O} < 1$) as a result of the primordial material from which the star forms, but the dredge-up process brings up carbon to the surface and in certain situations results in a carbon-rich envelope ($\text{C/O} > 1$). The creation of Carbon stars depends sensitively on the various physical processes shaping the evolution of AGB stars.

Despite these uncertainties, significant progress has been made in modeling AGB stars and their dust envelopes and incorporating those models in SPS models. On the stellar evolution side, AGB models are becoming increasingly realistic and constrained by observations (see Marigo et al. 2008; Girardi et al. 2010; Marigo et al.

¹ Department of Astronomy and Astrophysics, University of California, Santa Cruz, CA 95064, USA, avillaum@ucsc.edu

² Harvard-Smithsonian Center for Astrophysics, Cambridge, MA 02138, USA

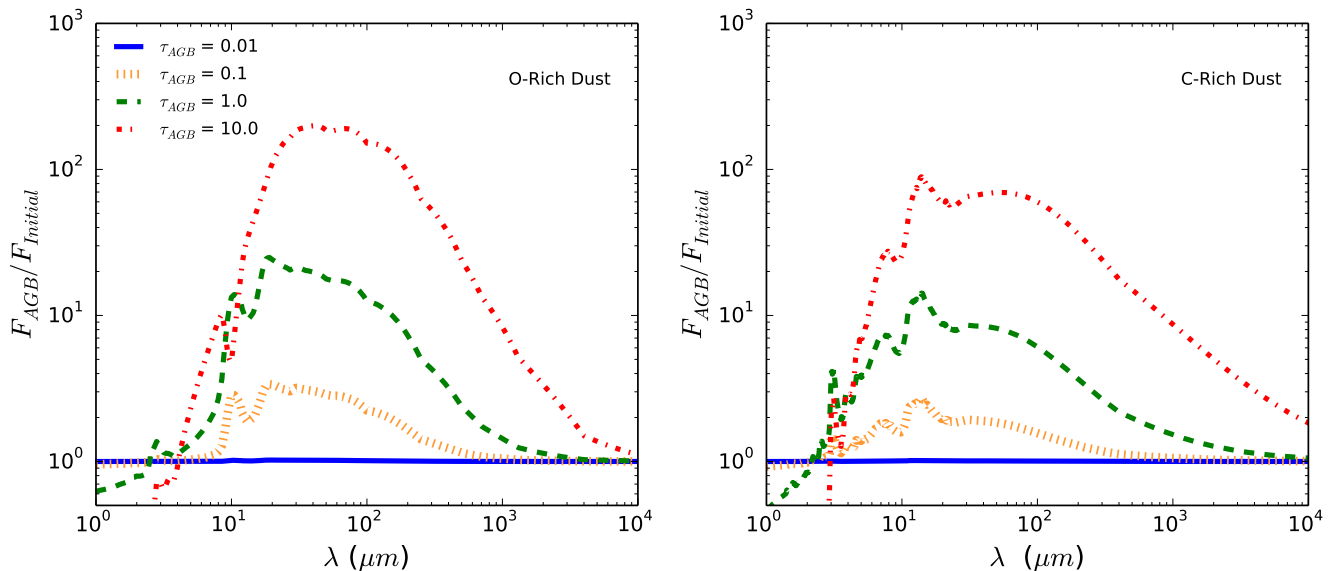


Figure 1. Ratio of the flux including circumstellar dust to the initial input spectra for various values of the dust optical depth at $1\mu\text{m}$, τ_{AGB} . The oxygen-rich models (left) are all for $T_{\text{eff}} = 2000$ K while the carbon-rich models (right) are all for $T_{\text{eff}} = 2400$ K. The dominant feature in the oxygen-rich grid is the silicate feature at $10\mu\text{m}$, seen in emission at moderate τ_{AGB} values and in absorption at high τ_{AGB} values. The silicon carbide feature at $11\mu\text{m}$ is the dominant feature in the carbon-rich grid which also becomes more prominent for larger values of τ_{AGB} .

2013; Cassarà et al. 2013; Rosenfield et al. 2014). There have also been advances in understanding the grain properties of dust around AGB stars from detailed observational studies (e.g. Suh 1999, 2000, 2002; Groenewegen 2006; Groenewegen et al. 2009, 2012; Srinivasan et al. 2011; Sargent et al. 2011).

The connection between stellar evolution models, which make predictions for the photospheric properties of stars, and the associated dusty circumstellar envelopes is complex and highly uncertain. Nonetheless, several efforts have been made to integrate circumstellar dust models into stellar isochrones and SPS models. Bressan et al. (1998) adopted various empirical (or empirically-motivated; see e.g., Vassiliadis & Wood 1993; Habing et al. 1994) relations between basic stellar parameters (i.e., mass, luminosity, and radius) and the mass-loss rate, pulsation period, velocity of the ejected material, and the optical depth of the circumstellar envelope. The basic approach of Bressan et al. (1998) has been updated and refined by Piovani et al. (2003), González-Lópezlira et al. (2010) and Cassarà et al. (2013).

The influence of AGB dust on the SEDs of galaxies is not well understood. Kelson & Holden (2010) and Chisari & Kelson (2012) suggested that dust from AGB stars may be the dominant contributor to the mid-IR light in star-forming galaxies. However, Melbourne & Boyer (2013) argued that the former studies overstated the effect of AGB stars on galaxies. In addition, the models of Silva et al. (1998) suggest that AGB dust plays a minor role in the SEDs of actively star-forming (and starburst) galaxies. In old stellar systems, it has been argued that the mid-IR shows evidence for dust around evolved stars (e.g., Athey et al. 2002; Martini et al. 2013). It is essential to understand these issues because the mid-IR is frequently used as a proxy for the star formation rate (SFR) in galaxies (e.g., Kennicutt & Evans 2012). However, the connection between mid-IR flux and SFR

may not be quite as simple as commonly assumed, especially for older stellar populations where heating of dust by older stellar populations (e.g., Salim et al. 2009; Utomo et al. 2014), and emission due to circumstellar dust around evolved stars (e.g. Martini et al. 2013) may play an important role. At $z \sim 2$, the *Spitzer* $24\mu\text{m}$ flux probes the rest frame $\sim 8\mu\text{m}$, and so understanding the contributions to the observed SEDs at $\sim 10\text{--}30\mu\text{m}$ is critical for deriving reliable SFRs. In addition, it has been suggested that the mid-IR emission associated with AGB stars could be employed as a stellar population age diagnostic (Bressan et al. 1998).

In this work we create models for the dusty circumstellar envelopes around AGB stars and include those models in the Flexible Stellar Population Synthesis (FSPS Conroy et al. 2009; Conroy & Gunn 2010) models. We employ the publicly available radiative transfer code DUSTY (Ivezic et al. 1999) to model the dusty envelopes and then an empirically motivated prescription to assign dust shells to AGB stars in isochrones.

The rest of paper is organized as follows: Section 2 details the modeling of circumstellar dust shells and how they are connected to isochrones. In Section 3 we test and calibrate the new dust models using IR data of the Large and Small Magellanic Clouds. In Section 4 we explore the parameter space of the models to see in which regimes the AGB dust has a significant influence on the integrated SEDs of composite stellar populations and compare the models to a variety of extragalactic data. Finally, in Section 5 we discuss the limits and implications of our results.

2. INCLUDING CIRCUMSTELLAR AGB DUST IN STELLAR POPULATION SYNTHESIS MODELS

2.1. Modeling Dusty Envelopes

We use the radiative transfer code DUSTY (Ivezic & Elitzur 1997; Ivezic et al. 1999) to model dusty cir-

Table 1
Summary of the parameters chosen as input for the DUSTY models

Parameter	Carbon-Rich	Oxygen-Rich
Photosphere Properties		
Photosphere Model	Aringer	BaSeL
T_{eff}	2400 – 4000 K	2000 – 4000 K
$\log g$	0.0	0.0
Metallicity	Z_{\odot}	Z_{\odot}
Envelope Properties		
R_{in} Temperature (T_c)	1100 K	700 K
Density Profile	r^{-2}	r^{-2}
Dust Grain Properties		
κ	$3200 \mu\text{m}^2 g^{-1}$	$3000 \mu\text{m}^2 g^{-1}$
Q_{ext}	0.1	0.1
Grain Size (a)	$0.1 \mu\text{m}$	$0.1 \mu\text{m}$
Density (ρ_d)	$2.26 g cm^{-3}$	$2.5 g cm^{-3}$

cumstellar shells around AGB stars. DUSTY solves the 1D radiative transfer equation for a source embedded in a dusty region assuming spherical symmetry. The input to DUSTY is straightforward — it requires an input spectrum, the dust properties (chemical composition, grain size distribution, the dust temperature at the inner boundary), a radial density profile, and the optical depth of the envelope at a reference wavelength. We altered the wavelength grid to be finer than the default (1968 wavelength points instead of 105). In this section we describe our choice of inputs and summarize those choices in Table 1.

We created two separate sets of models, one each for the carbon-rich and oxygen-rich AGB stars. In addition to composition, the models are a function of the optical depth, τ_{AGB} (herein this refers to optical depth at $1\mu\text{m}$), and the effective temperature of the star, T_{eff} . The model DUSTY spectra are implemented in the stellar population synthesis code differentially, in that only the ratio of the output to input spectra are stored and used within the code.

In Figure 1 we show the behavior of the oxygen-rich and carbon-rich grids as a function of optical depth at constant effective temperature for the carbon-rich and oxygen-rich grids. In this figure, we can see the characteristic features of the dust grains used in each set of models. For example, the $11\mu\text{m}$ feature caused by SiC in the carbon-rich grid (right) and the $10\mu\text{m}$ silicate feature in the oxygen-rich grid (left). The $10\mu\text{m}$ silicate feature varies from an emission to an absorption feature as a function of τ_{AGB} .

The differential implementation of the models allows us to keep the stellar parameters beyond effective temperature, such as stellar metallicity and surface gravity, constant. In Figure 2 we show the sensitivity of the differential spectra to surface gravity (middle panel) and metallicity (bottom panel). As can be seen, variations of these parameters does not have a significant impact on the differential spectrum. As such, surface gravity is kept constant at $\log(g) = 0.0$ and the metallicity at $Z = Z_{\odot}$ for both the carbon-rich and oxygen-rich differential spectra.

For the oxygen-rich input stellar spectra we use the

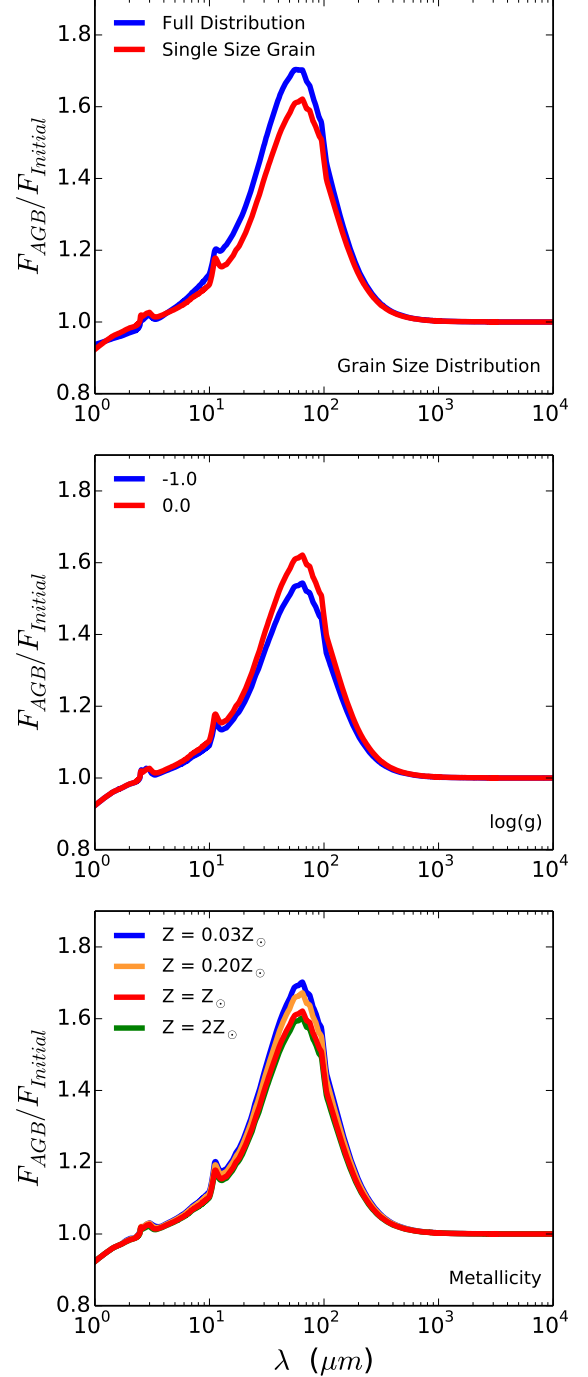


Figure 2. Ratio of the flux including circumstellar dust to the initial input spectra for different grain distributions (top), surface gravity values (middle), and metallicity (bottom) to demonstrate how sensitive the AGB dust models are to these values. The red line in each panel represents our fiducial input spectrum used in the grid with a chosen effective temperature of 3000 K, all models are for $\tau_{\text{AGB}} = 0.1$. The differential spectra are generally insensitive to varying the parameters of the input spectrum.

BaSeL (Lejeune et al. 1997) spectral library with effective temperatures ranging from 2000 K to 4000 K. For the carbon-rich models we use the Aringer (Aringer et al. 2009) spectral library with effective temperatures ranging from 2400 K to 4000 K. Stars hotter than $\sim 4000\text{K}$

Table 2
Dust condensation temperature (T_c)

	Carbon-Rich	Oxygen-Rich
This work	1100 K	700 K
Cassara et al. (2013)	1500 K	1000 K
Groenewegen et al. (2009a)	900-1200 K	900-1200 K
Groenewegen et al. (2009b) ^a	1000-1200 K	800-1000 K
Marigo et al. (2008)	800-1500 K	800-1500 K
Groenewegen (2006)	1000-1200 K	1000-1500 K
Piovan et al. (2003)	1000 K	1000 K
Lorenz-Martins & Pompeia (2001) ^a	-	417 - 1011 K
Suh (2000)	1000 K	-
Suh (1999)	-	700/1000 K ^b
Bressan et al. (1998)	1500 K	1000 K
David & Papoular (1990)	-	500 K - 800 K
Rowen-Robinson & Harris (1982)	-	500/1000 K

^a Values were fitted as part of a model

^b Suh (1999) mentions that both temperatures have been used in the literature but chooses 1000 K for their own models

are not expected to contain significant circumstellar dust shells.

A key characteristic of the dust is quantified through the value of the extinction coefficient, κ ,

$$\kappa = \frac{n_d \pi a^2 Q_{\text{ext}}}{\rho_d}, \quad (1)$$

where Q_{ext} is the extinction efficiency factor, a is the grain size, ρ_d is the internal grain density, and n_d is the spatial number density of a particular grain species in a dust mixture. The final κ for each grain mixture is the sum of the κ values for each component in that mixture. We fix $Q_{\text{ext}} = 0.1$ throughout, motivated by Suh (1999), and the grain densities are adopted from Bressan et al. (1998) (See Table 1).

Throughout this work we adopt a grain size distribution that is a delta function at $0.1 \mu\text{m}$. This is a common, though rather simplistic assumption (e.g., Suh 1999, 2002; Piovan et al. 2003). We tested the impact of adopting different grain size distributions in the DUSTY models and found that we can obtain similar emergent SEDs for different grain size distributions by varying τ_{AGB} (see top panel of Figure 2).

In our model the parameters κ , the dust-to-gas ratio, and R_{in} depend on whether the star is oxygen-rich or carbon-rich. To compute κ we need to assume a certain dust composition. It is not currently possible to compute κ from first principles owing to various uncertainties such as the detailed properties and evolution of circumstellar dust shells and dust grain formation and destruction processes, although efforts along these lines are currently ongoing (e.g., Jones et al. 2012, Ventura et al. 2014, Nanni et al. 2013, Schneider et al. 2014, Dell’Agli et al. 2014).

As Cassarà et al. (2013) discuss in detail, we expect the dust composition to change as a function of τ_{AGB} . In principle, this would require us to compute κ and τ_{AGB} iteratively (Piovan et al. 2003). However, AGB stars can have diverse features from one another and it is unlikely that any one set of uniform models will fit all AGB stars equally. Since we have no a priori model for how the grain properties should vary with stellar properties, we choose to adopt a relatively simple, observationally motivated scheme.

Sargent et al. (2010) and Srinivasan et al. (2010) fit models to multi-wavelength broadband photometry of AGB stars with grain composition as a free parameter of the model. For oxygen-rich stars, Sargent et al. (2010) found that a grain composition of 100% oxygen-deficient silicates was sufficient to fit the data. However, as an oxygen-rich shell becomes more optically thick we expect the silicates to become colder (Suh 1999 and Suh 2002). Therefore, in our grid we adopt a grain type that varies with τ_{AGB} . In our grid, for oxygen-rich stars we use warm silicates for the dust composition up until $\tau_{\text{AGB}} = 3$ when we start to include cold silicates in the mixture. The grain densities, sizes, and Q_{ext} parameters are all kept constant between the warm and cold silicates. For this reason, the extinction coefficient (Equation 1) remains the same as the grid transitions from cold to warm silicates.

For carbon-rich stars, Srinivasan et al. (2010) found that a mixture of amorphous carbon (amC) and 10% silicon carbide (SiC) was sufficient. These dust compositions were used for their entire grid of AGB dust models, GRAMS (Sargent et al. 2011 and Srinivasan et al. 2011). Furthermore, we found that changing the amC and SiC ratio made only a modest difference in our results so we decided to keep the grain mixture for carbon-rich stars constant at 90% amC and 10% SiC for all values of τ_{AGB} .

Despite the simplicity of our dust compositions we find that they are sufficient for modeling individual AGB stars. We demonstrate this in Figure 3 where we show how the DUSTY models compare to the SEDs of well-studied AGB stars HV 5715, SSTISAGE1C J052206.92, LPV 28579, and CW Leo. For the first three stars the data is as presented in Sargent et al. (2010) and Srinivasan et al. (2010) with *UBVI* (Zaritsky et al. 1997, Magellanic Clouds Photometric Survey), *JHK* (Skrutskie et al. 2006, 2 Micron All Sky Survey), *Spitzer* IRAC and MIPS bandpasses (Meixner et al. 2006, SAGE), and *Spitzer* IRS spectroscopy (Kemper et al. 2010, SAGE-Spec). CW Leo is an extensively observed object. Here we fit optical to IR photometry (as presented in Groenewegen et al. 2012) – *gri* (Ahn et al. 2012, Sloan Digital Sky Survey), *VRI* (Le Bertre 1987), *JHKLM* (Le Bertre 1992), IRAS (Beichman et al. 1988), AKARI (Ita et al. 2008, AKARI IRC Survey of the Large Magellanic Cloud), and SPIRE and PACS bandpasses (Groenewegen et al. 2011, Mass-Loss of Evolved Stars).

HV 5715, SSTISAGE1C J052206.92, LPV 28579, and CW Leo are all oxygen-rich AGB stars and LPV 28579 is carbon-rich. Sargent et al. (2011) presented detailed models of HV 5715 and SSTISAGE1C J052206.92, Srinivasan et al. (2011) modeled LPV 28579, and Groenewegen et al. (2012) modeled CW Leo. The models used in Figure 3 were made using the default parameters of our model grid and only allowing T_{eff} and τ_{AGB} to vary. The shape of the observed SEDs and the observed features are fit well by the models. This comparison provides a test of our model grid both as a function of T_{eff} , τ_{AGB} , and whether the star is oxygen or carbon-rich. We emphasize however that these fits are not unique and there are many degeneracies between e.g., the shell density profile, τ_{AGB} , grain size distribution, etc.

The temperature of the dust at the inner radius, R_{in} , of the shell, T_c , is an important source of uncertainty in the modeling. Table 2 summarizes the different values for T_c

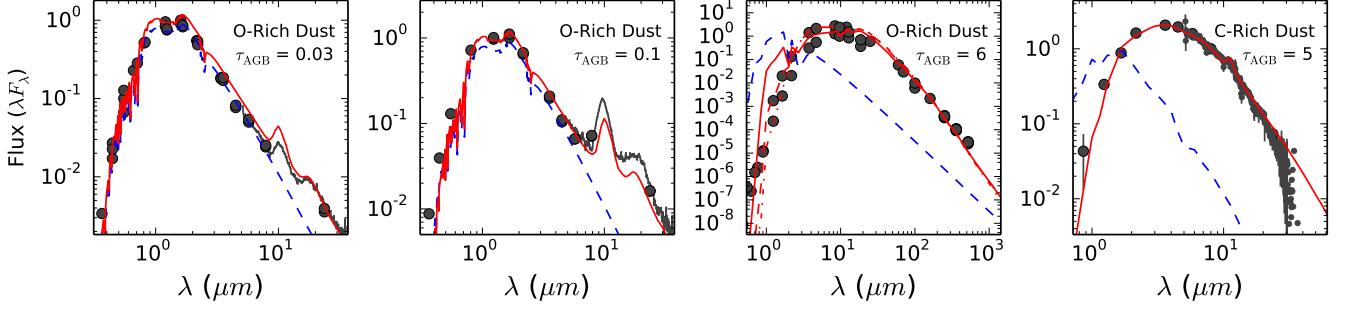


Figure 3. By-eye fits to four AGB stars using radiative transfer models. The blue dashed line is the input stellar photosphere and the red line shows the effect of including a circumstellar dust shell. The normalization in each panel is arbitrary. Far left: M star HV5715 with $T_{\text{eff}} = 3500\text{K}$ and a grain composition of 100% warm silicates. Middle left: M star SSTISAGE1C J052206.92 with $T_{\text{eff}} = 3500\text{K}$ and grain composition of 100% warm silicates. Middle right: M star CW Leo with $T_{\text{eff}} = 2000\text{K}$; this star is very dust enshrouded and so we adopt a grain composition of 100% cold silicates. Different lines are plotted showing different values of the dust temperature at the inner boundary, T_c . We show $T_c = 700\text{K}, 1000\text{K}, 1300\text{K}$ (see text for details). There is a general agreement of the models for different T_c values especially at the mid-IR wavelengths. Far right: Carbon star LPV 28579 with $T_{\text{eff}} = 3200\text{K}$.

adopted in the literature and demonstrates the range of values considered by various authors. Our choice for T_c was based on fitting the data from Martini et al. (2013) (as presented in Section 4).

We compared the dust models of individual stars for the different T_c values to the stars shown in Figure 3 to check that on an individual basis the values gave reasonable agreement to AGB stars. In Figure 3 we compare the different models for the range of T_c values to CW Leo. Since CW Leo is the most dust enshrouded AGB star of our sample any effects due to changes to the input parameters will be amplified compared to the other stars in the sample. These comparisons lead us to adopt $T_c = 700\text{K}$ for the oxygen-rich grid. We emphasize that T_c could in principle vary with stellar type (i.e., with T_{eff}), metallicity, etc., and our choice of a constant value for T_c may introduce systematic uncertainties in the final model results.

The grid and the code used to generate the grid are publicly available³.

2.2. Connecting Dusty Envelopes to Stellar Isochrones

With grids of circumstellar AGB dust emission as a function of optical depth, T_{eff} , and C/O taken from the dustless isochrones, our goal now is to connect the grids to stellar isochrones by computing the value of τ_{AGB} at each isochrone point.

The optical depth, τ_{AGB} , is the key quantity that connects the stellar parameters provided by the isochrones to the models of the dust shells. Computing τ_{AGB} from stellar parameters has been discussed extensively in the literature beginning with the work of Vassiliadis & Wood (1993) and Habing et al. (1994). Subsequent work by Bressan et al. (1998), Piovan et al. (2003), and Casarà et al. (2013) refined this technique to incorporate dusty envelopes into their SPS codes. In this work, we largely follow these previous efforts in coupling circumstellar dust models to stellar isochrones. We will be brief in our description of computing τ_{AGB} as the former three papers provide extensive details of the derivations of the following equations.

³ <https://github.com/AlexaVillaume/AGBGrid>
commit: 7308b5c424268c16da3e4ae9aef0b5f0bfcfa6

We start with an initial equation for τ_{AGB} that is derived assuming spherical symmetry and by integrating over the thickness of the shell while assuming that $R_{\text{out}} \gg R_{\text{in}}$, where R_{out} and R_{in} are the outer and inner radii of the dust envelope:

$$\tau_{\text{AGB}} = \frac{\delta \dot{M} \kappa}{4\pi v_{\text{exp}} R_{\text{in}}} \frac{1}{R_{\text{in}}} \quad (2)$$

In Vassiliadis & Wood (1993) they used observationally estimated mass-loss rates of Galactic Mira variables and OH/IR stars to empirically determine equations for \dot{M} , pulsation period (P), and v_{exp} :

$$\frac{v_{\text{exp}}}{\text{km s}^{-1}} = -13.5 + 0.056 \frac{P}{\text{days}}, \quad (3)$$

with an additional condition that v_{exp} lie in the range of $3 - 15 \text{ km s}^{-1}$, and:

$$\log \frac{P}{\text{days}} = -2.07 + 1.94 \log \frac{R}{R_{\odot}} - 0.9 \log \frac{M}{M_{\odot}} \quad (4)$$

The equations for \dot{M} are a function of initial mass of the star and whether the star is in a super-wind phase, defined by Vassiliadis & Wood (1993) as stars with $P > 500$ days. When not in the super-wind phase the mass-loss rate for a star with an initial mass $< 2.5 M_{\odot}$ is described by a simple relation with pulsation period,

$$\log \dot{M} = -11.4 + 0.0123P, \quad (5)$$

where P is in days, and \dot{M} is in $M_{\odot} \text{ yr}^{-1}$, and for stars with initial mass $> 2.5 M_{\odot}$,

$$\log \dot{M} = -11.4 + 0.0125 \left[P - 100 \left(\frac{M}{M_{\odot}} - 2.5 \right) \right] \quad (6)$$

In the super-wind phase the mass-loss rate is described as,

$$\dot{M} = \frac{1}{c v_{\text{exp}}} \frac{L}{L_{\odot}} \quad (7)$$

where c and v_{exp} are in units of km s^{-1} .

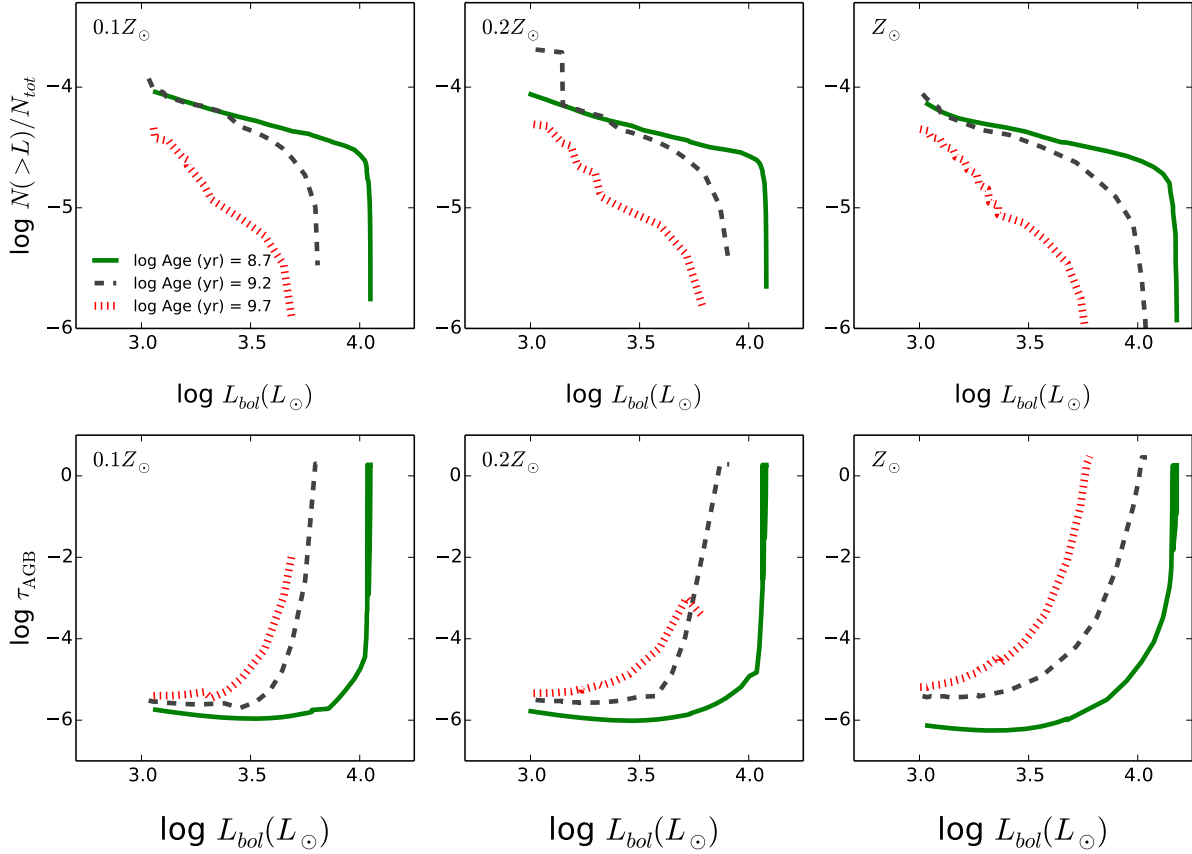


Figure 4. Top Panels: Cumulative luminosity functions for AGB stars for different ages and metallicities. Bottom Panels: Value of τ_{AGB} as a function of L_{bol} , age, and metallicity. Only stars with $L_{\text{bol}} \geq 10^3 L_{\odot}$ are shown. Stars that have the highest τ_{AGB} values, i.e. the most dust-enshrouded, have the greatest bolometric luminosity, but are rare.

The inner radius, R_{in} , is derived by equating the stellar luminosity with the luminosity at the inner radius, remembering that the inner radius is defined as the radius where the temperature is equal to the dust condensation temperature, T_c ,

$$R_{\text{in}} = \left[\frac{L}{4\pi T_c^4} \right]^{\frac{1}{2}}. \quad (8)$$

We adopt our T_c values from Table 2 to obtain a final relation for carbon-rich stars,

$$R_{\text{in}} = 1.92 \times 10^{12} \left(\frac{L}{L_{\odot}} \right)^{\frac{1}{2}} \text{ cm}, \quad (9)$$

and for oxygen-rich stars,

$$R_{\text{in}} = 4.74 \times 10^{12} \left(\frac{L}{L_{\odot}} \right)^{\frac{1}{2}} \text{ cm}. \quad (10)$$

The dust-to-gas ratio, δ , is obtained by inverting the observed correlation between it and v_{exp} found in Habing et al. (1994),

$$\delta = \frac{\delta_{\text{AGB}} v_{\text{exp}}^2}{225} \left(\frac{L}{10^4 L_{\odot}} \right)^{-0.06}, \quad (11)$$

where we adopt $\delta_{\text{AGB}} = 0.01$ for oxygen-rich stars (Suh 1999) and $\delta_{\text{AGB}} = 0.0025$ for carbon-rich stars (Blanco

et al. 1998). Note that in the following we assume that δ does not depend on metallicity. See Section 2.3 for details.

With the above equations we can now explore the behavior of τ_{AGB} along the isochrones as a function of metallicity and age. This is shown in Figure 4 where we show the number of AGB stars as a function of luminosity (top) and their corresponding τ_{AGB} values (bottom). In this figure we see that the knee of the luminosity functions coincide with the upturn of the τ_{AGB} values. This indicates that brighter stars are both rarer and have larger values of τ_{AGB} . Only for these rare stars is there an appreciable level of dust obscuration.

The models are now included in the FSPS population synthesis code (Conroy & Gunn 2010) as of v2.5.⁴ FSPS computes τ_{AGB} as per the equations above for identified AGB stars in the isochrones. With τ_{AGB} , T_{eff} , and the composition of the stellar envelope, FSPS interpolates within the grid of DUSTY models and grafts the interpolated model onto the stellar SED.

We briefly review here the salient characteristics of the FSPS stellar population synthesis model. FSPS takes as input a set of stellar isochrones (here we use the Padova models detailed in Marigo et al. (2008)), stellar spectral libraries (in our case the BaSeL library), allows the user to specify a stellar initial mass function (IMF), and outputs simple stellar populations (SSPs), and, if a star

⁴ code.google.com/p/fpsps

formation history is specified, composite stellar populations. FSPS includes models for diffuse dust absorption and emission. The model has been extensively calibrated and tested against observations, see Conroy & Gunn (2010) for details.

When AGB dust is turned on in FSPS, τ_{AGB} is computed at each isochrone point using the method described above. Fundamentally, τ_{AGB} depends on the mass and age of the star.

2.3. Metallicity Dependence of the Dust-to-Gas Ratio?

To first order, the seed elements relevant for grain formation in oxygen-rich environments, such as O, Si, and Fe, will vary in proportion to the metallicity of the star. It therefore might seem reasonable for the dust-to-gas ratio to increase linearly with the metallicity of the star (e.g., Habing et al. 1994).

However, recent models attempting to follow the formation and dust grains self-consistently as a function of AGB mass and metallicity have revealed a complicated relation between the dust-to-gas ratio and metallicity (e.g. Ferrarotti & Gail 2006). Schneider et al. (2014) detailed the complicated factors that contribute to the dust production of AGB stars by comparing the observed dust production rates of AGB stars in the Large and Small Magellanic Clouds to theoretical models. Schneider et al. (2014) noted that efficiency of the Hot Bottom Burning (HBB), the TDU, and the mass of the star all contribute to the efficiency of the dust production for AGB stars. And, as Ventura et al. (2014) noted, the efficiency of these mechanisms are influenced by the modeling of convection in the star. Discrepancies between the theoretical dust yields and observed dust yields found in Schneider et al. (2014) highlight that we do not have a solid predictive model for dust formation in AGB winds. Moreover, current models suggest that dust production could be a complex, non-monotonic function of metallicity. For these reasons we decided to adopt a simple approach and keep the dust-to-gas ratio fixed for all oxygen-rich stars, independently of metallicity.

For carbon-rich stars the seed elements for the grains (carbon) are made in-situ in the star, so one would expect that the dust-to-gas ratio to have little dependence on the original metallicity of the star. Hence also for carbon-rich stars we keep the dust-to-gas ratio fixed, independent of metallicity.

3. CALIBRATING STELLAR POPULATION MODELS THAT INCLUDE AGB DUST

As an initial test of the new models, we compare them with the photometry of the Large Magellanic Cloud (LMC) and the Small Magellanic Cloud (SMC). The data is from the Survey of the Agents of Galaxy Evolution (SAGE) survey (Meixner et al. 2006 for LMC data and Gordon et al. 2011 for SMC). The SAGE survey is based on Spitzer IRAC and MIPS data, including photometry in [3.6], [4.5], [5.8], and [8.0] bands.

For the LMC data we follow Cassarà et al. (2013) and select a region within π square degrees of the center of the LMC (RA = 5h23m.5, DEC = -69,45'). For the [3.6] - [8.0] vs [8.0] color-magnitude diagram (CMD) for both galaxies we make a further cut on the dim, red background objects for clarity. In Figure 5 we include isochrones for both the LMC and SMC, with respec-

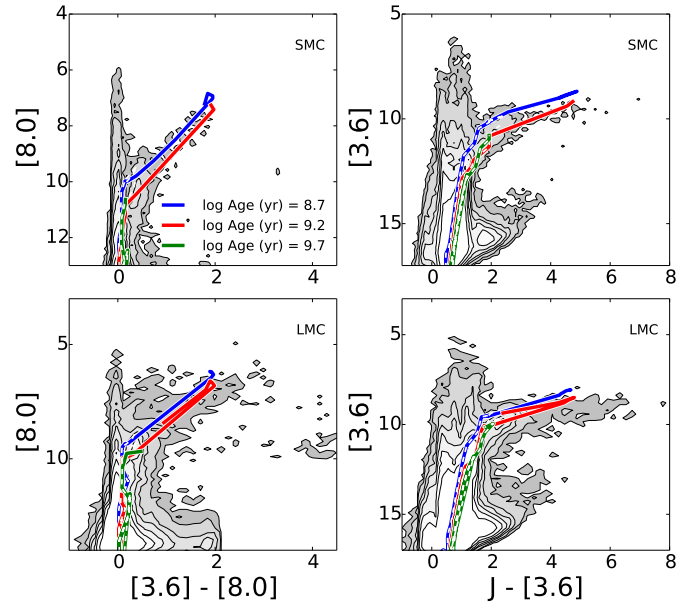


Figure 5. Color magnitude diagrams of stars in the Small Magellanic Cloud (top) and the Large Magellanic Cloud (bottom) overlaid with SSP models of various ages. Foreground objects have been removed with a color-magnitude cut. The solid lines are single-age models that include AGB circumstellar dust while the dashed lines show the same models without AGB dust. Note that the luminous red spur in the data is only captured by the models that include AGB dust.

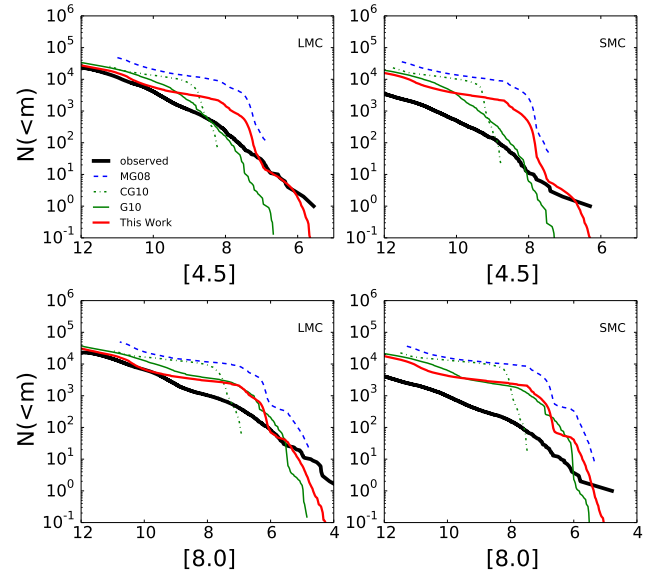


Figure 6. Comparison of the observed and model luminosity functions for the SMC and LMC. Model LFs were derived using the default Padova 2008 isochrones (Marigo et al. 2008), the updated Padova isochrones by Girardi et al. (2010) (Case A), isochrones as calibrated by Conroy & Gunn (2010), and isochrones calibrated for this work. All model predictions include circumstellar dust for AGB stars and have been convolved with estimated SFHs of the LMC and SMC.

tive metallicities of $Z = 0.008$ and $Z = 0.004$, from the Padova stellar models.

In Figure 5 there are six models in each panel: three ages, and for each age there are models both with and without AGB dust (solid and dashed lines, respectively).

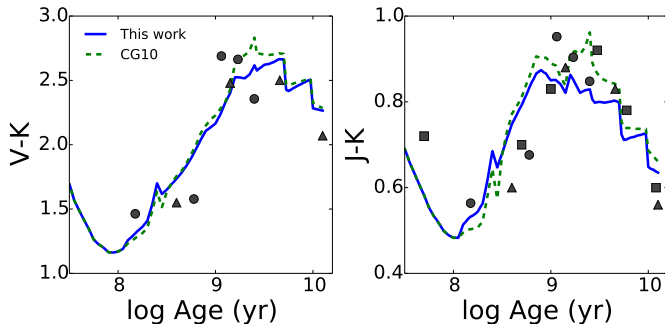


Figure 7. SSP colors as a function of age, comparing models from this work to those described in Conroy & Gunn (2010). This figure also includes LMC star cluster data from Noël et al. (2013) (circles), Pessev et al. (2008) (triangles), and González et al. (2004) (squares). By construction, the colors predicted by the calibrations described in this work are very similar to the colors from Conroy & Gunn (2010). Notice that the very similar integrated light colors between the two models nonetheless produce very different LFs in Figure 6.

Overall, the models with circumstellar dust cover the observed behavior of both the LMC and SMC, providing support to our method for assigning dusty envelopes to AGB stars in isochrones (see also Cassarà et al. (2013) who find similar agreement with a different set of AGB dust models).

Comparing isochrones to data in CMD space hides potentially significant discrepancies in the relative numbers of stars in different evolutionary phases. We provide a closer comparison of our models to LMC and SMC luminosity functions (LFs) in Figure 6. The observed cumulative LFs (thick black line in Figure 6) are constructed from the catalogs of Boyer et al. (2011), including only those stars classified as any variety of O, C, or x-AGB. We have inspected images of the brightest objects to insure that they are not strongly affected by confusion or high backgrounds.

We create model LFs by convolving model isochrones with measured SFHs and metallicity histories from Harris & Zaritsky (2004) and applying a cut of $T_{\text{eff}} < 4000$ K to isolate the AGB stars. We checked that the convolution of the SFHs with the stellar mass and integrated luminosities reproduces the observed integrated NIR light of the clouds and the total stellar masses reported by Harris & Zaritsky (2004) and Harris & Zaritsky (2009) to within a factor of two. We show four models in Figure 6, three of which differ only in the input isochrones: unaltered Padova isochrones (Marigo et al. 2008) (MG08, dashed blue line), re-calibrated Padova isochrones from Conroy & Gunn (2010) (CG10, dot-dashed green line), and a new normalization created specifically to provide a better fit to the observed LF (solid red line, described in detail below). The fourth is computed from the updated Padova isochrones as described in Girardi et al. (2010) (Case A). We emphasize that this is an entirely different model where we adopt the Girardi et al. (2010) bolometric corrections and Marigo et al. (2008) dust models. In all cases circumstellar dust around AGB stars has been included.

Uncertainties in the SFHs are difficult to incorporate correctly due to the substantial covariance between the SFRs in adjacent temporal bins, but the uncertainties on the SFR in any given bin are typically less than a factor

of two, and this gives an upper limit on the uncertainties in the predicted CLFs at any magnitude. The effects of photometric uncertainties on the predicted CLFs are negligible, though uncertainties substantially larger than reported may affect the bright end.

The predicted luminosity functions determined from the Marigo et al. (2008) isochrones and the Conroy & Gunn (2010) calibrations do not match the data well. Models based on the Marigo et al. (2008) isochrones over-predict the number of AGB stars while models based on the Conroy & Gunn (2010) normalization do not span the full extent of the magnitude range. Due to these shortcomings we decided to introduce updated calibrations of the Padova isochrones for the AGB phase, different from those presented in Conroy & Gunn (2010).

Conroy & Gunn (2010) chose to decrease the overall contribution of AGB stars to the integrated light by decreasing $\log L$ and slightly modifying T_{eff} . This modification resulted in a better fit to the NIR colors of intermediate age star clusters in the LMC. For the new calibration, we chose to keep $\log L$ unchanged and instead adjust the IMF weight to effectively reduce the lifetimes of AGB stars:

$$\text{weight} = \max(+0.1, 10^{-1.0+(t-8.0)/2.5}), \quad (12)$$

$$\text{IMF}'_{\text{weight}} = \text{weight} \times \text{IMF}_{\text{weight}}, \quad (13)$$

where t is \log age (yr). This change keeps the integrated light predictions similar to the original Conroy & Gunn (2010) normalization (see Figure 7 and below). This new calibration is the default re-normalization for Padova isochrones in FSPS as of v2.5. The calibration introduced in this work is an improvement from previous versions available in FSPS.

The dusty isochrones from Girardi et al. (2010) are comparable to the models presented in this work. There is a difference in the extent in magnitude that two models span seen at $4.5\mu\text{m}$. At $8.0\mu\text{m}$, however, the overall shape of the luminosity functions are similar. We compared all the dust schemes made available by the Padova group and found none that made an improvement the magnitude range in the Girardi et al. (2010) models. The model LMC luminosity function presented in this work is well-matched to the data with the exception of the bump seen at $7 < [8.0] < 9$.

However, while improved from previous versions, the model SMC luminosity function still significantly over-predicts the number of AGB stars. The source of this discrepancy is currently unclear but it could be a problem with the treatment of the AGB evolution in the lower metallicity isochrones. Agreement between the models and data for the SMC in Figure 5 indicates that we are likely not over-predicting the amount of AGB dust per L_{bol} but, again, the CMDs hides information regarding AGB lifetimes which are critical for the luminosity functions in Figure 6. Given that a similar over-prediction is seen in the Girardi et al. (2010) models indicates that this is an issue more fundamental than the dust models.

As a further check, we compare predicted AGB number counts for several galaxies from the ACS Nearby Galaxy Survey Treasury (ANGST Dalcanton et al. 2009) using the HST WFC3 F160W filter. Melbourne et al. (2012)

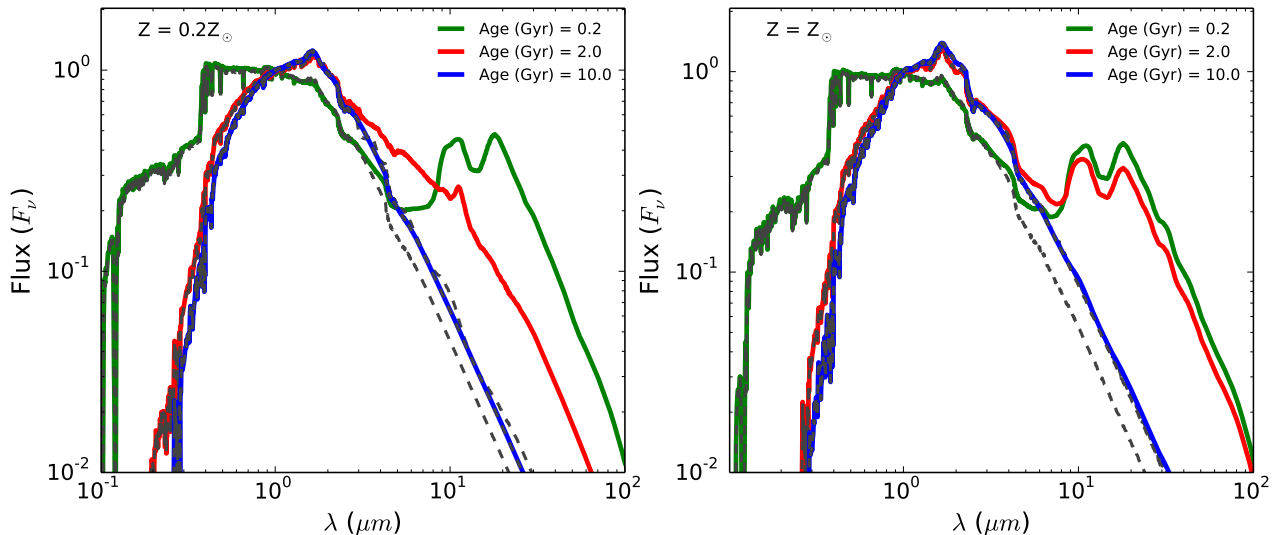


Figure 8. Model spectral energy distributions as a function of age comparing models with (solid lines) and without (dashed lines) circumstellar dust around AGB stars. Notice that circumstellar dust has a very large effect on the SED for $\lambda \gtrsim 4\mu\text{m}$. For the Padova stellar models that we employ, the effect of circumstellar dust around AGB stars is relatively modest at 10 Gyr.

Table 3
Comparison of AGB counts for ANGST galaxies

Galaxy	Observed	MG08	G10	This Work	$\frac{\text{ThisWork}}{\text{Data}}$
DD078	273	858	721	724	2.65
DD082	1046	2556	1122	1709	1.63
IC2574-SGS	1504	2587	1554	1867	1.24
NGC4163	640	1425	677	945	1.47
UGC4305-1	740	1438	1113	1136	1.54
UGC4305-2	721	1532	1063	1428	1.98

compared the observed number of AGB stars for ANGST galaxies to the predictions by the (Marigo et al. 2008, MG08) isochrones and the (Girardi et al. 2010, G10) modifications to them. We present those, along with our models that include the updated normalization of the AGB lifetimes in Table 3. As expected, our model predictions are lower than those of MG08. However, there are still cases where the discrepancy with observations is significant, as noted in Melbourne et al. (2012) when adopting the more recent G10 isochrones. Our mean model-data number ratio for AGB stars is 1.75, similar to the value from Melbourne et al. (2012) when using the G10 isochrones.

Our new normalization of the Padova isochrones was chosen to provide a decent fit to both the LMC luminosity function and the integrated colors of LMC star clusters. The latter is shown in Figure 7. In this figure we compare both our new normalization and the normalization from CG10 to observations (See Figure 2, Conroy & Gunn 2010). The latter are obtained by stacking star clusters in bins of age to reduce the effects of sparse sampling of the AGB in individual clusters. By construction, the integrated colors are well-matched to the data.

While we have calibrated our models based on Figure 7, we note that Girardi et al. (2013) cautioned about biases introduced due to a “boosting” of the number of AGB stars right at the age of many LMC clusters. However, the good agreement between the observed and

model LMC LF indicates that the effect of AGB boosting over a narrow range of ages is unlikely to have a significant effect on our results.

We wish to emphasize that our renormalization of the Padova isochrones is completely ad hoc and is simply chosen to provide better fits to observations. Definitive conclusions regarding AGB lifetimes, etc., will require actual modifications to the underlying physics in the stellar models, as for example done in Girardi et al. (2010).

4. THE EFFECT OF AGB DUST ON INTEGRATED LIGHT

4.1. General Trends

In this section we first describe the general conditions in which circumstellar dust may affect the integrated light of simple and complex stellar populations (§4.1), then move to discussing two examples in which there is evidence for the impact of circumstellar dust (early-type galaxies in §4.2 and low-metallicity dwarf galaxies in §4.3), and one example in which circumstellar dust appears to play no important role (actively star-forming galaxies, in §4.4).

With the new circumstellar dust models we can calculate revised SEDs and compare them to models without circumstellar dust. In Figure 8 we show model SEDs with (solid lines) and without (dashed lines) dust shells around AGB stars for ages of 0.2, 2, and 10 Gyr for $Z = 0.2Z_\odot$ and $Z = Z_\odot$. The circumstellar dust substantially increases the model flux red-ward of $\sim 4\mu\text{m}$. At old ages the influence of the AGB dust is sharply diminished, having little discernible impact on the SED. We note here that the models in this figure contain no diffuse dust associated with the interstellar medium (see below).

The trends with age and metallicity in Figure 8 can at least partially be understood by considering separately the effects of carbon-rich and oxygen-rich stars on the integrated SED. We explore this in Figure 9, which shows the fractional contribution of oxygen-rich and carbon-rich stars to L_{bol} (top panels) and the relative contribu-

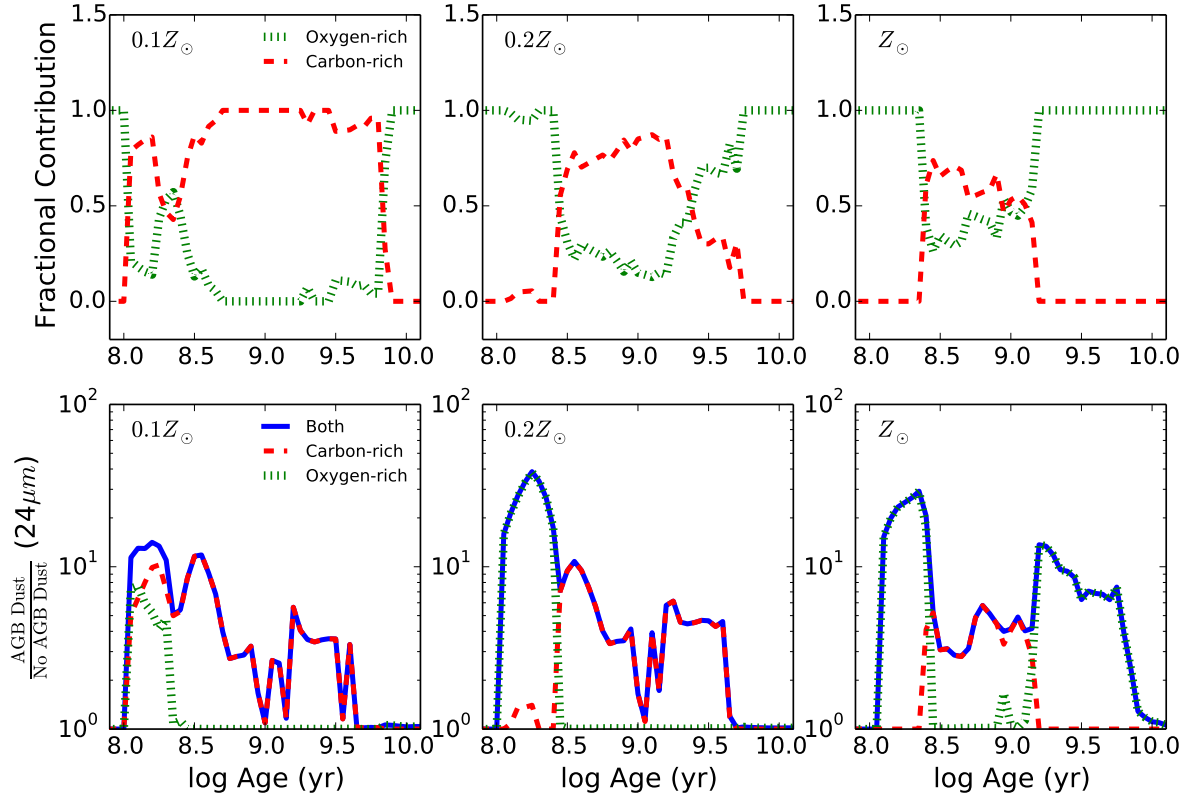


Figure 9. Relative contributions of carbon and oxygen-rich stars to the integrated light of single-age stellar populations. Top Panel: Fractional contribution of carbon and oxygen-rich stars to the total bolometric AGB luminosity. Bottom Panel: Relative contribution to total $24\mu\text{m}$ flux, comparing models with and without AGB dust. This figure highlights both the age and metallicity dependence of carbon-rich star formation and also the disproportional influence of carbon-rich stars to the mid-IR flux when AGB dust is included in the models.

tion of oxygen-rich and carbon-rich stars to the $24\mu\text{m}$ flux (bottom panels). Note that we are using Padova stellar models here.

We see the well-known fact that the appearance of carbon-rich stars is both metallicity and age dependent. In the top row of Figure 9 we see that for the lowest metallicity model, $Z = 0.1Z_{\odot}$, carbon-rich stars dominate L_{bol} for a longer period of time than the higher metallicity models. Moreover, carbon-rich stars do not exist at old ages, $9.3 \lesssim \log t/\text{yr} \lesssim 10$ for high metallicities. The age dependence is complicated, depending on processes such as the TDU and HBB. Detailing when and under what conditions carbon-rich stars are produced is outside the scope of this work but it is a much discussed subject in the literature (e.g., Iben & Renzini 1983; Di Criscienzo et al. 2013, and the references therein). It is important to understand because at certain ages and metallicities carbon-rich stars are dustier and therefore redder than oxygen-rich stars, as demonstrated in the lower panels of Figure 9. We see in Figure 9 that carbon-rich stars have a disproportionate influence on the $24\mu\text{m}$ flux relative to their overall L_{bol} contribution. The lack of carbon-rich stars at old ages, combined with the generally lower AGB luminosities at late times (see Figure 4) explains why circumstellar dust emission from AGB stars has a relatively modest effect on the integrated light SED at old ages.

In Figure 10 we show how AGB dust affects the NIR and mid-IR integrated light of composite stellar population models as a function of age for different metallicities (note that this refers to populations as a whole, rather than the metallicity of individual stars discussed in §2.1, which will have an effect on the SPS models), star formation histories (SFHs; represented by exponential models with an e-folding time given by τ_{SF}), and diffuse dust content (the contribution of dust around young stars and dust in the ISM). In this figure four wavelength ranges are shown and in each panel we compute the ratio of luminosities between models with and without circumstellar AGB dust.

The diffuse dust model is a combination of the Charlot & Fall (2000) model for dust attenuation, with a power-law attenuation curve (with τ_{diff} quoted at 5500\AA and the power-law index, $\alpha = -0.7$ unless stated otherwise) and the Draine & Li (2007) model for diffuse dust emission. The overall amount of diffuse dust emission is determined by energy conservation. In this paper, models that include diffuse dust also include dust around young stars, the so-called “birth cloud component”, where $\tau_{\text{bc}} = 3\tau_{\text{diff}}$. Note that the Draine & Li (2007) dust models include both thermal emission from cold dust and PAH emission. The models are described by three parameters q_{PAH} , U_{min} , γ . Unless otherwise stated we adopt 3.5%, 1.0, 0.01 respectively for these

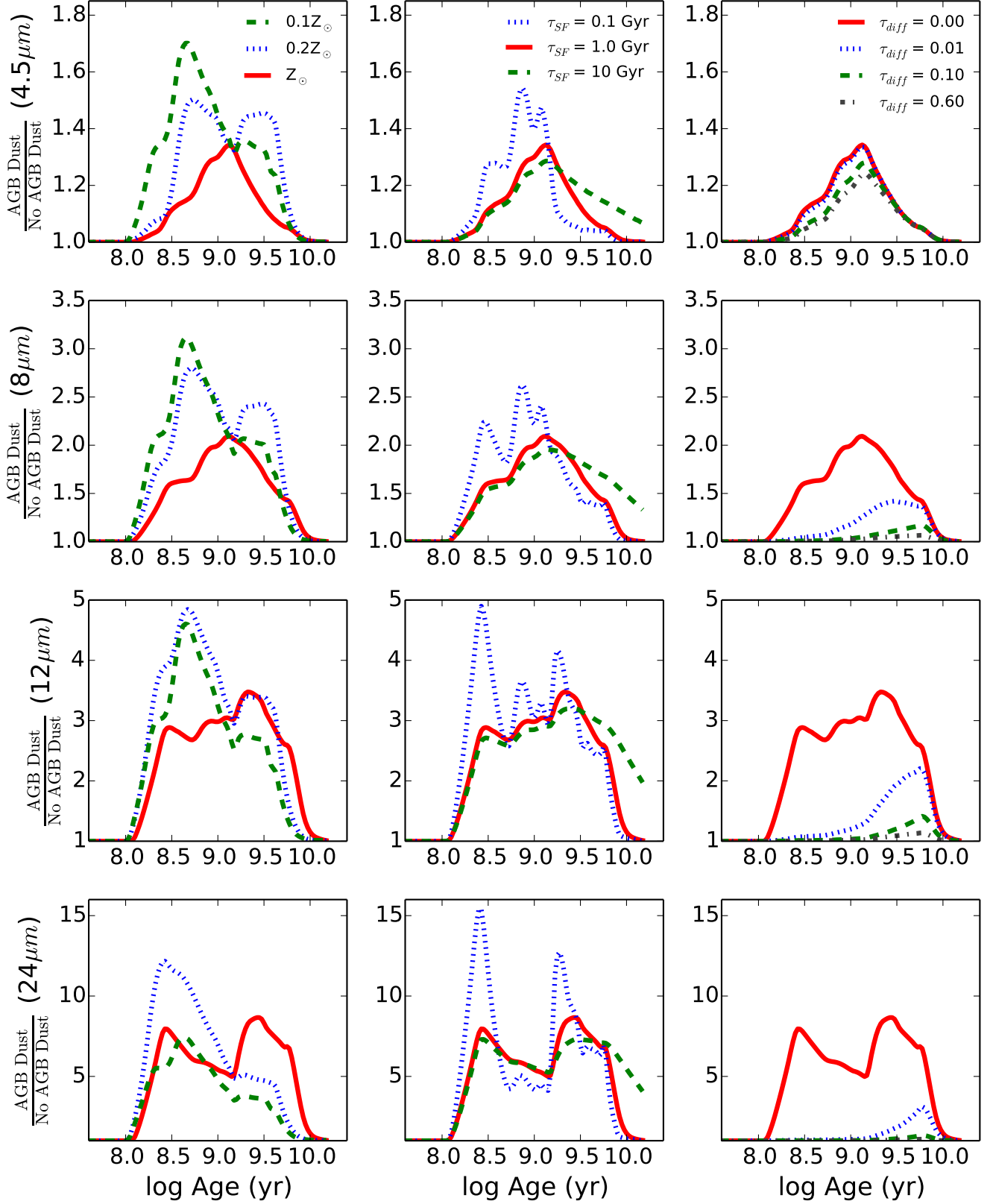


Figure 10. Effect of circumstellar dust on model fluxes as a function of metallicity (left column), star-formation history (middle column), diffuse dust content (right column), and wavelength (top to bottom). The model plotted in red is the default model, same across every panel, with $Z = Z_{\odot}$, $\tau_{SF} = 1$ Gyr, and $\tau_{diff} = 0.0$. The diffuse dust content significantly reduces the influence of AGB circumstellar dust at $\gtrsim 8\mu m$ but at $4.5\mu m$ the models are largely insensitive to the presence of diffuse dust.

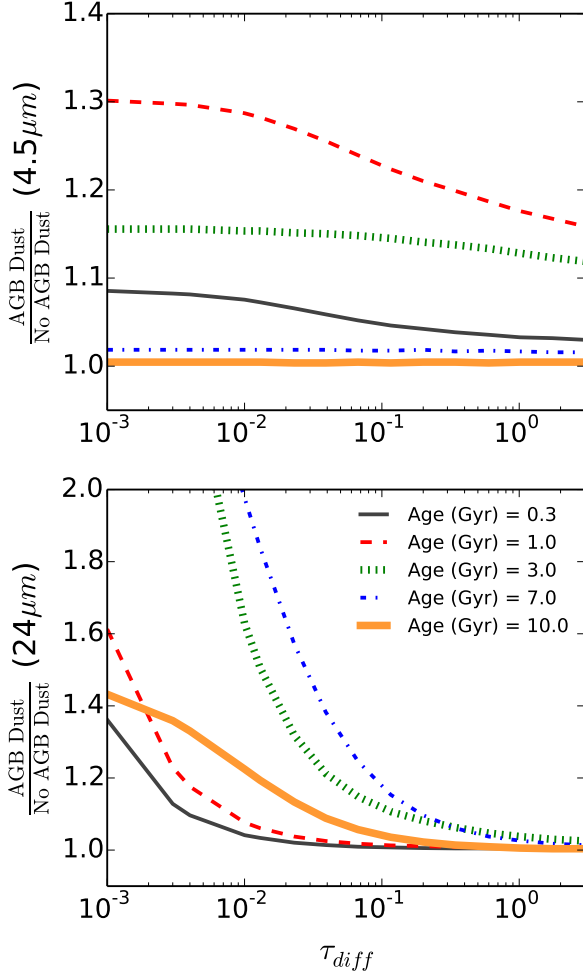


Figure 11. A more detailed look at the effect of diffuse dust on the contribution of AGB dust at $4.5\mu\text{m}$ (top) and $24\mu\text{m}$ (bottom) for several ages. At $24\mu\text{m}$ there is dramatic decline in the influence of AGB dust for even moderate values of diffuse dust. However, flux at $4.5\mu\text{m}$ is largely insensitive to the contributions of diffuse dust as the diffuse dust in our model is not hot and therefore does not radiate substantially at such short wavelengths.

values.

We see in all models that only after ~ 0.1 Gyr does AGB dust become influential, peaking at about 1 Gyr, with a significant reduction by the time the galaxy reaches 10 Gyr in age. The influence of AGB dust on the SED varies in interesting ways as a function of wavelength, metallicity, and SFH, but by far the most influential parameter is the amount of diffuse dust.

For galaxies where there is no diffuse dust the impact of the dust around AGB stars is significant and extends to wavelengths as short as $\sim 4\mu\text{m}$. However, even a modest amount of diffuse dust significantly diminishes the relative influence of AGB dust at $\gtrsim 8\mu\text{m}$. At shorter wavelengths the effect of AGB dust dominates over that of diffuse dust, since in our model the diffuse dust component is generally not hot enough to emit significantly at $< 8\mu\text{m}$. We investigate this in more detail in Figure 11 where we show the effect of AGB dust at $4.5\mu\text{m}$

and $24\mu\text{m}$ as a function of the amount of diffuse dust for several ages. At $4.5\mu\text{m}$ the AGB flux is relatively insensitive to the diffuse dust content but at $24\mu\text{m}$ the diffuse dust greatly reduces the influence of the emission from the AGB dust shells. From $\sim 1.0 - 10.0$ Gyr the AGB dust has a significant influence of the mid-IR light only for low diffuse dust values and, consistent with the previous figures, drops off as the diffuse dust becomes more prominent. We therefore conclude that circumstellar dust around AGB stars will be important in regimes where the diffuse dust optical depth is roughly $\lesssim 0.1$.

We also investigate the effect of AGB dust on optical-NIR and NIR-mid-IR colors in Figure 12. The difference is not large for $V - K_s$, but this color is commonly employed in high-precision SED modeling of galaxies and so even a small change could potentially induce large differences in derived parameters. The models that include AGB dust tend to be bluer in $V - K_s$ than models that do not for a range of metallicities and ages. This is because AGB stars, with or without dust shells, contribute essentially zero flux in the V band and significant flux in K_s . Dusty AGB stars can be optically thick even in the K_s band, resulting in a lower flux and hence bluer $V - K_s$ color. In the middle and bottom panels of Figure 12 we see that the models with AGB dust are significantly redder than models without for optical-mid-IR and mid-IR-mid-IR colors.

4.2. Comparison To Early-Type Galaxies

Early-type galaxies are potential candidate systems where the effect of AGB dust may be important, owing to their generally low diffuse dust content. They are known to host intermediate and old age populations, $1 < t < 10$ Gyr, based on optical absorption line spectroscopy (e.g. Trager et al. 1998; Thomas et al. 2005; Jimenez et al. 2007; Trager et al. 2005; Thomas et al. 2005; Conroy et al. 2014). While many early-type galaxies do show evidence for diffuse dust at low levels (e.g. Lauer et al. 2005), the origins of which are actively debated, there exists galaxies with only upper limits in the FIR, suggesting that they have very little diffuse dust (e.g. Jura et al. 1987; Knapp et al. 1989; Temi et al. 2009; Martini et al. 2013).

Athey et al. (2002) presented a mid-IR spectrum from the Infrared Space Observatory (ISO) for the early-type galaxy NGC 1404. These authors found a clear excess in the data at $8 - 14\mu\text{m}$ compared to a blackbody extrapolation. They attributed this excess to O-rich AGB features. In Figure 13 we show their data for NGC 1404 compared to our models with no dust (blue line) and three models with AGB dust for different ages (red lines). All models assume the galaxy has a metallicity of Z_\odot .

First, we see that by including AGB dust in the model the fits to the data are greatly improved at $8 - 12\mu\text{m}$. Furthermore, we see from the three models with AGB dust the mid-IR can be a powerful age discriminator, as already discussed in Bregman et al. (2006), Bressan et al. (1998), and Athey et al. (2002), for simple systems with only one burst of star-formation. We find that a model with AGB dust and an age of ~ 7.5 Gyr provides the best fit to the $10\mu\text{m}$ feature. This is in good agreement with the 9 Gyr estimated by Bregman et al. (2006), who used the AGB dust models from Piovan et al. (2003) to estimate galaxy ages based on mid-IR SEDs. This age

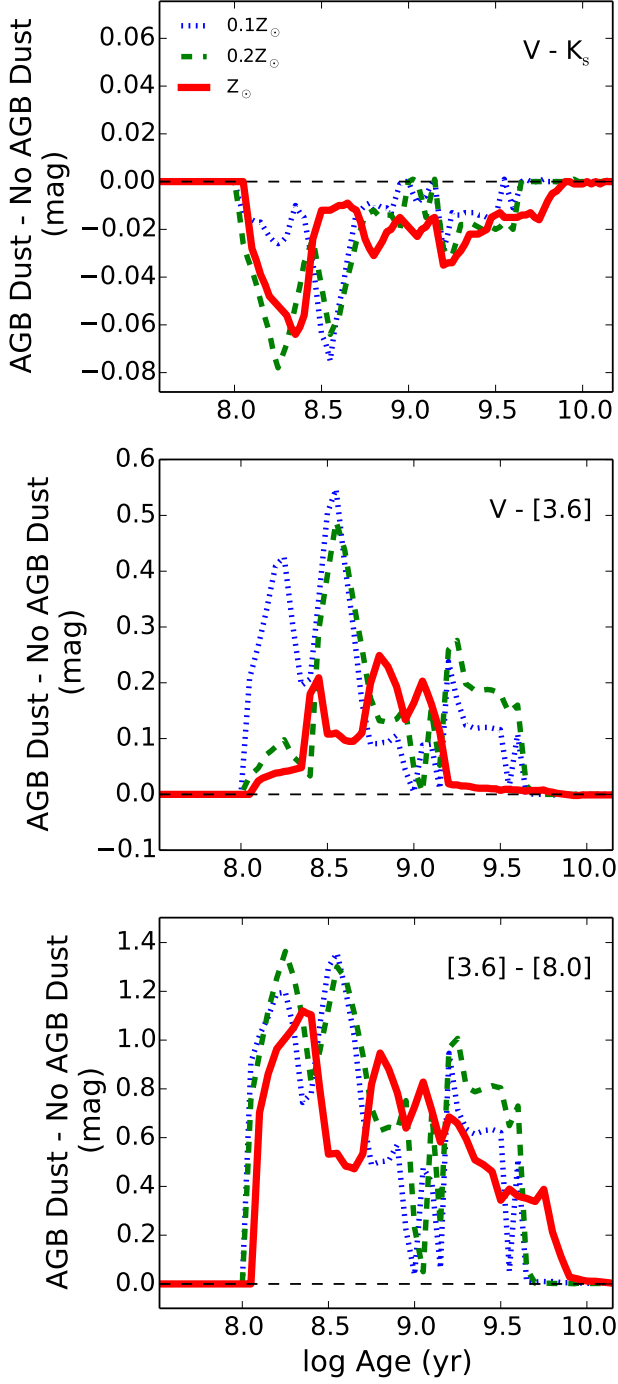


Figure 12. Effect of AGB dust on optical and NIR colors. The effect on mid-IR colors is large and very time- and metallicity-dependent. The contribution of circumstellar AGB dust to $V-K_s$ is small compared to the other colors, but $V-K_s$ is frequently used in high-precision SED modeling of galaxies and, with the typically small measurement uncertainties of optical-NIR colors, the relatively small effect of circumstellar dust on $V-K_s$ may in fact have a significant effect on parameters derived from SED modeling.

is also in agreement with an optical spectroscopically-estimated age for this galaxy of 7 Gyr (Conroy & van Dokkum, in prep).

Interpretation of the mid-IR data for NGC 1404 is complicated by the fact that this galaxy is apparently not

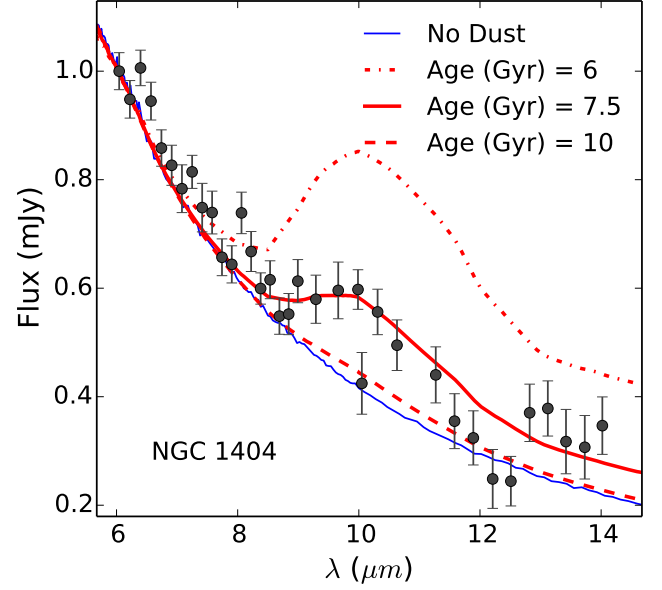


Figure 13. ISO spectroscopy for the early-type galaxy NGC 1404 (points with errors), compared to models with (red) and without (blue) AGB dust. The model with AGB dust gives a much better fit to the data at $> 8\mu m$. Moreover, it is clear that the mid-IR is very sensitive to age even over the interval 6 – 10 Gyr.

entirely devoid of diffuse dust. It is detected by Herschel at $70\mu m$ and $160\mu m$ (Temi et al. 2009), indicating the presence of cold dust. However, we attempted to fit the data from Athey et al. (2002) with only diffuse dust (no AGB dust) and found that such a model could not simultaneously fit the mid-IR and FIR data (see also Figure 15). Therefore, we conclude that circumstellar AGB dust appears to be necessary to fit the mid-IR data for this galaxy.

Martini et al. (2013) recently published mid-IR photometry of early-type galaxies from *Spitzer*'s IRAC and MIPS bands. Martini et al. (2013) divided the sample based on whether there were diffuse dust lanes detected in HST imaging and detected at 70 and $160\mu m$. Rampazzo et al. (2013) also published an atlas of mid-IR spectroscopy from *Spitzer*-IRS of early-type galaxies that they sort into classifications based on the contribution of old stellar populations to the mid-IR continuum, where class 0 are galaxies where the old stellar populations are most significant.

In Figure 14 we compare the data for galaxies that did not have detected dust lanes and were classified as class 0 in Rampazzo et al. (2013) to models that include (solid-red) and do not include (dashed-blue) AGB dust. All models plotted were made for a solar metallicity, single-age stellar population. The data were normalized to the flux at $5.72\mu m$, which should eliminate aperture size issues between IRAC and IRS. The ages of the galaxies were estimated by hand to provide a satisfactory fit to the $3 - 20\mu m$ data. The model that includes AGB dust fits the $3.6 - 8.0\mu m$ data just as well as the model that does not, only for $\geq 8.0\mu m$ are there significant differences between models with and without circumstellar dust (for these ages). The models provide a good fit to the mid-IR spectra from *Spitzer*-IRS. In particular, the overall shape, from $5 - 20\mu m$, is reproduced well and the relative strength and positions of the broad 10 and $18\mu m$

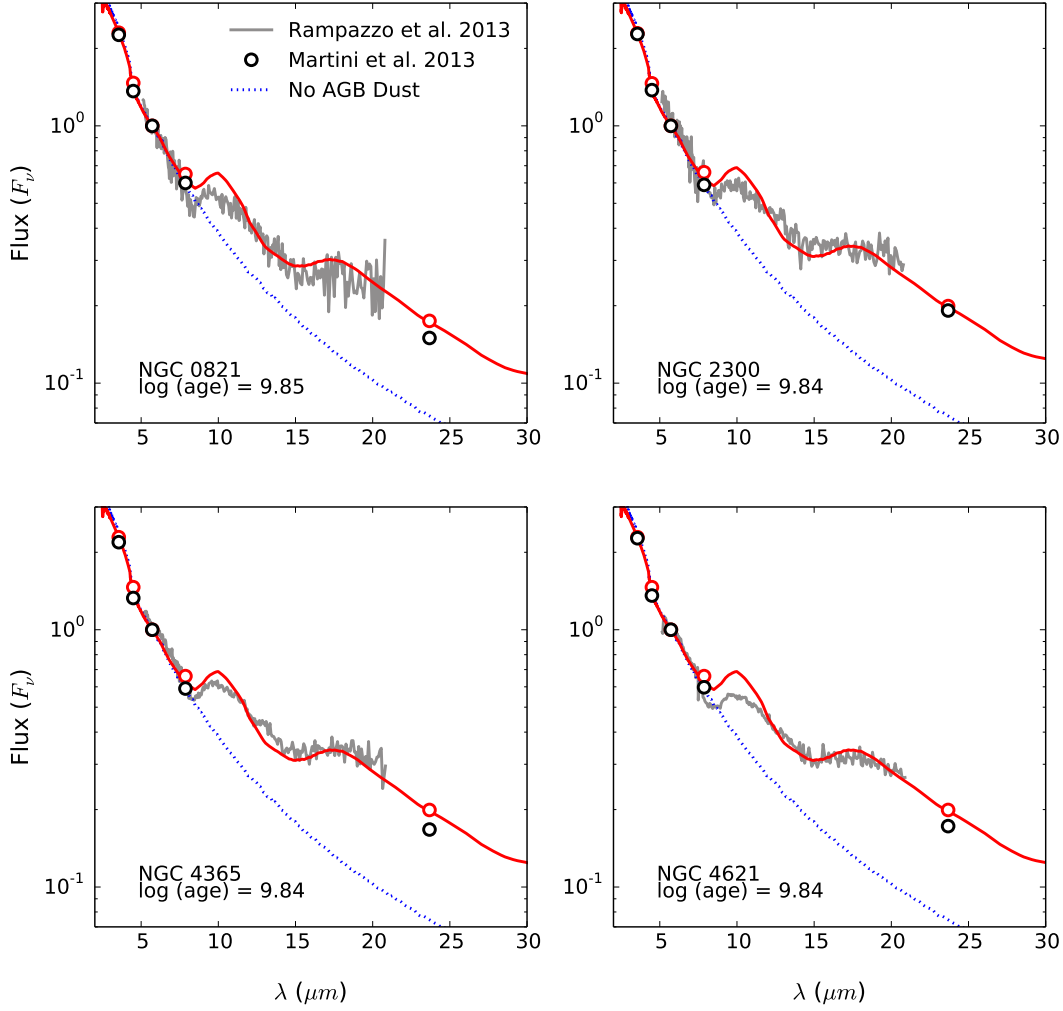


Figure 14. *Spitzer* IRAC and MIPS photometry and IRS spectroscopy of a sample of early-type galaxies compared to $Z=Z_{\odot}$ models with (red) and without (blue-dashed) AGB dust. Photometry are from Martini et al. (2013) and spectra are from Rampazzo et al. (2013). All data were normalized to $5.72 \mu\text{m}$, the IRAC 3 central wavelength. The errors in the photometry are smaller than the points. The ages were determined through by-eye fits. The models that include AGB dust generally fit the data well, with slight over predictions of the the $10\mu\text{m}$ emission feature seen in all the spectra.

dust features are generally well matched.

In Figure 15 we compare the observations of NGC 2300 with both the AGB dust model and two models that includes only diffuse dust. The fundamental difference between the latter two models is the adopted value of q_{PAH} . In one case we adopt the fiducial value while in the other we adopt an unreasonably high value of 10%⁵. We added as much diffuse dust into the models as possible without exceeding the constraints of the FIR flux at $70\mu\text{m}$ and $160\mu\text{m}$. It is clear that the model with only diffuse dust cannot reproduce the $8 - 24\mu\text{m}$ features seen in early-type galaxies with influential old stellar populations. Varying the diffuse dust parameters q_{PAH} and U_{min} does not qualitatively improve the fits.

The slight over prediction of the strength of the $10\mu\text{m}$

emission feature is likely due to our treatment in the dust grain properties. We reiterate that our grain scheme is relatively simplistic and there is an abundance of evidence that the actual grain mixtures in AGB stars, and their dependence on the properties of the star, are more complicated than represented in the models presented here (e.g. Jones et al. 2012; McDonald et al. 2010). Other groups producing similar dust shell models have incorporated more detailed approaches to the grain schemes. For example, Cassarà et al. (2013) detail a sophisticated approach to the grain mixtures that accounts for changes in τ_{AGB} and \dot{M} and Groenewegen (2006) include aluminum oxide dust along with the more standard silicate in oxygen-rich AGB stars. In future work we will explore the effect of different grain species on the mid-IR spectra of early-type galaxies.

⁵ This is an extrapolation of the Draine & Li (2007) models, the highest value Draine & Li (2007) compute is 4.58%.

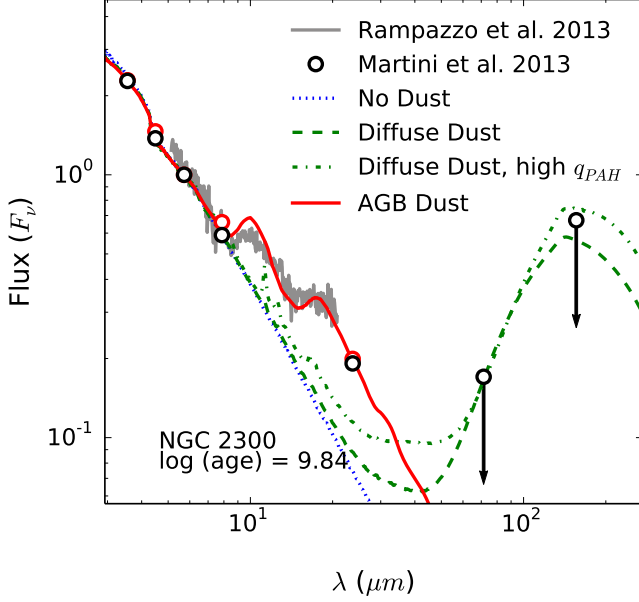


Figure 15. Same as the upper-right panel in Figure 14 but with two models with only τ_{diff} included. The dashed represents the standard diffuse dust model with $\tau_{\text{diff}} = 0.001$. The dot-dashed line represents an otherwise standard model but with the q_{PAH} parameter set at the highest allowable value, 10%, and $\tau_{\text{diff}} = 0.003$. The diffuse dust values were chosen to be as large as possible without exceeding the constraints placed $70\mu\text{m}$ and $160\mu\text{m}$ upper limits. It shows that diffuse dust does not fit the 6- $12\mu\text{m}$ features seen in galaxies like NGC 2300 i.e. early-type galaxies with dominant old age stellar populations.

4.3. Comparison to Low-Metallicity Galaxies

Low-metallicity galaxies are another class of objects in which circumstellar dust may significantly contribute to the integrated SED owing to their generally low diffuse dust content. Johnson et al. (2013) compared observations for a subset of ANGST galaxies with SPS models. They found and discussed the possible causes of a 0.2 dex under-prediction by the models compared to *Spitzer* data from the LVL survey presented in Dale et al. (2009) (see Figure 5 in Johnson et al. 2013). They considered the possibility that circumstellar dust around AGB stars, not included in the SPS models, may be the source of the discrepancy.

In Figure 16 we plot the offset between observed IRAC $8\mu\text{m}$ and MIPS $24\mu\text{m}$ magnitudes and predicted magnitudes for models with (blue squares) and without (red circles) AGB dust as a function of metallicity. For about half the galaxies, the metallicities are well constrained by nebular emission lines (Berg et al. 2012). For the rest of the sample, metallicities are estimated the mass-metallicity relationship (Berg et al. 2012; Lee et al. 2006); the resulting metallicities that are broadly consistent with those estimated from HST CMDs (Weisz et al. 2011). For each galaxy, the corresponding model has the same SFH and metallicity. The model photometry for each galaxy is based on the estimated SFH for each galaxy derived from CMDs; see Johnson et al. (2013) for details. The default models do not contain any diffuse dust.

In both panels we include linear fits to both sets of offsets; in general the offset is reduced with the inclusion

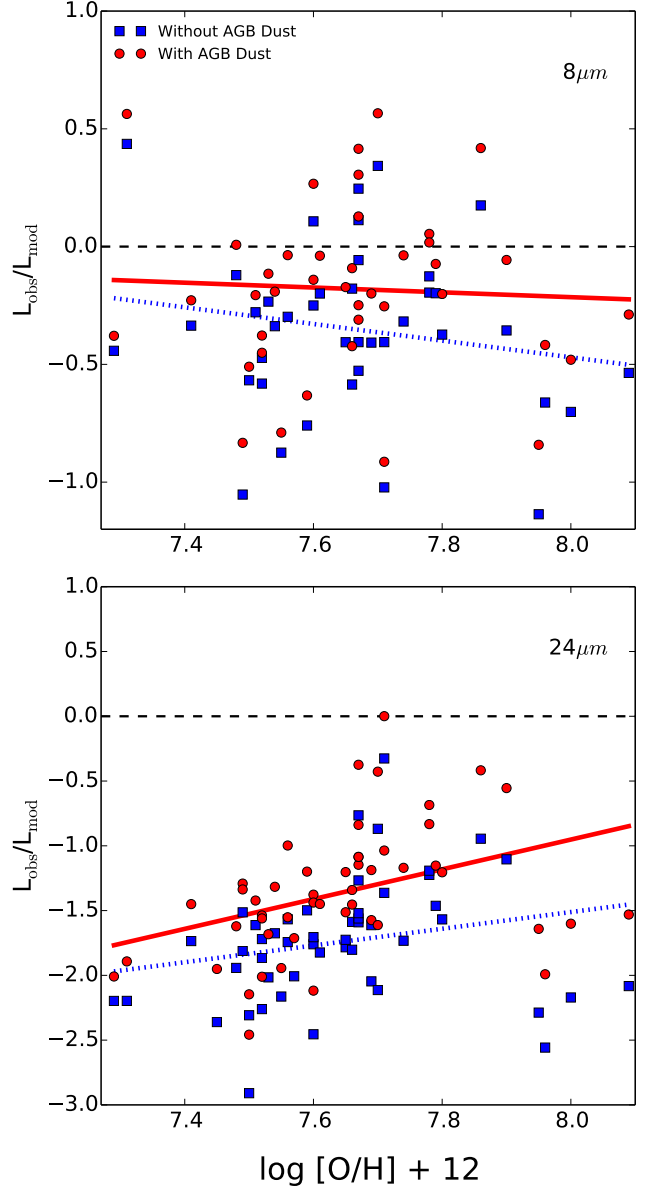


Figure 16. Comparison of the differences between observed and model magnitudes for low-metallicity dwarf galaxies from the ANGST survey. Results are shown for models both with and without circumstellar dust around AGB stars. The integrated light model predictions utilize the CMD-based SFHs for the ANGST galaxies. The lines plotted in each panel are linear fits to the points. The average difference between observed and model magnitudes is nearly zero for the $8\mu\text{m}$ flux but only slightly reduces the tension at $24\mu\text{m}$.

of AGB dust. For the $8.0\mu\text{m}$ flux, the average difference between observations and models is close to zero. However, for the $24\mu\text{m}$ flux, while there is some improvement in the offset in all the galaxies, a significant discrepancy remains even after including AGB dust.

We see a very strong correlation between metallicity and the size of the offsets at $24\mu\text{m}$. The origin of the correlation is unclear to us. In Figure 17 we compare the residuals between the observations and models that only include circumstellar AGB dust and models that include AGB dust and diffuse dust at $24\mu\text{m}$ ($q_{\text{PAH}} = 0.05$ and dust attenuation index $\alpha = -1.3$). We see that

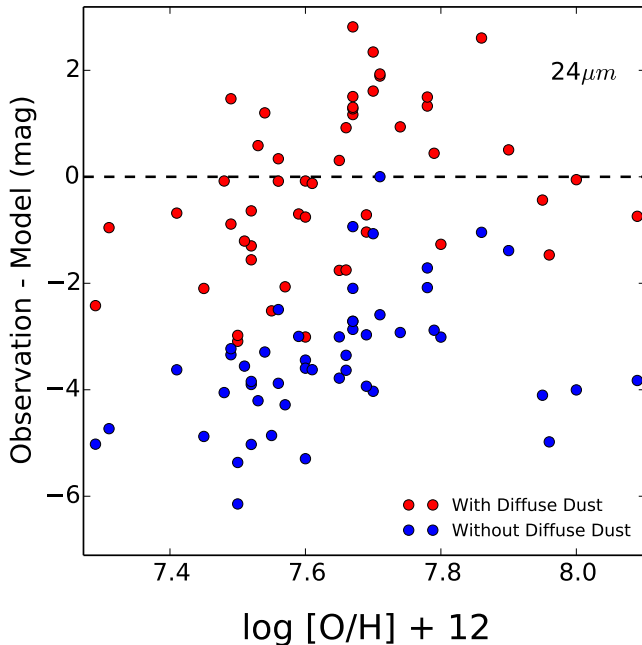


Figure 17. Comparison of the residuals between the predicted and observed $24\mu\text{m}$ magnitude for the low-metallicity ANGST galaxies as a function of metallicity. The addition of diffuse dust ($\tau_{\text{diff}} = 0.05$, red points) helps resolve the residuals that persist after including only circumstellar AGB dust (blue points), indicating that diffuse dust is important in these galaxies.

by including diffuse dust we are able to better capture the $24\mu\text{m}$ flux. However, the correlation with metallicity remains. This indicates that joint modeling of UV-IR SEDs is necessary for these galaxies to fully understand their characteristics.

4.4. Comparison to Star-Forming Galaxies at $z \sim 1$

Finally, we consider the effect of circumstellar dust on the SEDs of actively star-forming galaxies.

Kelson & Holden (2010) suggested that AGB stars may be responsible for a substantial fraction of the mid-IR luminosities in galaxies from $z = 0$ to $z = 2$. In Figure 18 we show color-color diagrams of galaxies at $z \sim 1$ from the FIREWORKS catalog, see Wuyts et al. (2008) for details (also, see Figure 2 from Kelson & Holden 2010). In each panel we include three models: a model with the standard amount of AGB dust (“ $1\times$ AGB dust”) where the amount of AGB dust included in the model is as described in §2.2; a model with a much larger amount of AGB dust (“ $100\times$ AGB dust”) where we multiplied the standard dust optical depth by 100, and a model with no AGB dust but a modest amount of diffuse dust ($\tau_{\text{diff}} = 0.05$). Each model assumes $Z = Z_{\odot}$, $\tau_{\text{SF}} = 2.0$ Gyr, and uses a delayed τ -model to be as similar as possible with the models from Kelson & Holden (2010). In the first panel we see no difference among the different models. This is expected since only optical colors are plotted and no dust will effect the flux at these wavelengths. This plot serves as a check that the models we have adopted are a reasonable description of the data and that they span the full range of optical-optical colors.

The second panel is an optical-mid-IR color-color plot and we see significant differences among the models. The standard AGB model is able to reproduce only a small

fraction of the galaxy colors but fails to span the whole extent of the color range. Even when boosting the AGB dust optical depth by a factor of 100 (far beyond what is plausible) we are unable to reproduce the full color range of the data. Furthermore, reducing the metallicity of the model to $Z = 0.4Z_{\odot}$ and thereby increasing the number of carbon stars (see Figure 9), and hence the MIR flux, only modestly improves the fits of the model to the data. However, a modest amount of diffuse dust can readily explain the full range of mid-IR colors. It therefore seems unlikely that AGB dust alone can explain the full range of the mid-IR colors.

This issue has also been discussed in Melbourne & Boyer (2013) where they compared the mid-IR colors of AGB stars in the SMC and LMC with the colors of AGB stars adopted for the models presented in Kelson & Holden (2010). Melbourne & Boyer (2013) concluded that the average AGB color adopted by Kelson & Holden (2010) were significantly redder than the observed average AGB colors. This is due to the fact that Kelson & Holden (2010) used heavily dust enshrouded AGB stars as representative of more typical AGB stars. Furthermore, Kelson & Holden (2010) used the Maraston (2005) stellar population models, which appear to assign too much weight to the TP-AGB phase (Kriek et al. 2010; Zibetti et al. 2012).

The results of this section are consistent with our findings from §4.1 as well as the findings of Melbourne & Boyer (2013). Actively star-forming galaxies generally contain significant quantities of diffuse dust that tends to overwhelm the effect of circumstellar dust in the mid-IR.

5. DISCUSSION

In this work we computed a set of empirically-calibrated radiative transfer models for the dusty circumstellar shells around AGB stars. These models were coupled to a stellar population synthesis code in order to explore under what circumstances AGB dust might impact the integrated SEDs of composite stellar populations (i.e., star clusters and galaxies). The models indicate that AGB dust will play an important role in shaping observed SEDs of both quiescent and star-forming galaxies when $4\mu\text{m} \lesssim \lambda \lesssim 8\mu\text{m}$. At longer wavelengths, the influence of AGB dust will be substantial only when the diffuse dust content is low ($A_V \lesssim 0.1$). These conclusions are in good agreement with the results of Silva et al. (1998), who included both circumstellar dust around AGB stars and diffuse dust in their SED models.

Modeling the contribution of dusty circumstellar shells to the integrated light of stellar populations carries a number of uncertainties that are presently difficult to quantify. These include the lifetimes, luminosities, mass-loss rates, and compositional changes of AGB stars, the structure, extent, and lifetime of the circumstellar shell, the types and quantity of dust within the shell, and the optical properties of dust grains. We attempted to calibrate and/or mitigate these uncertainties by tuning the model to match several key observables include the SEDs of oxygen and carbon-rich stars, the morphology of the color-magnitude diagram of the LMC and SMC, the luminosity function of stars in the LMC and SMC, and the numbers of AGB stars in low metallicity galaxies from the ANGST survey.

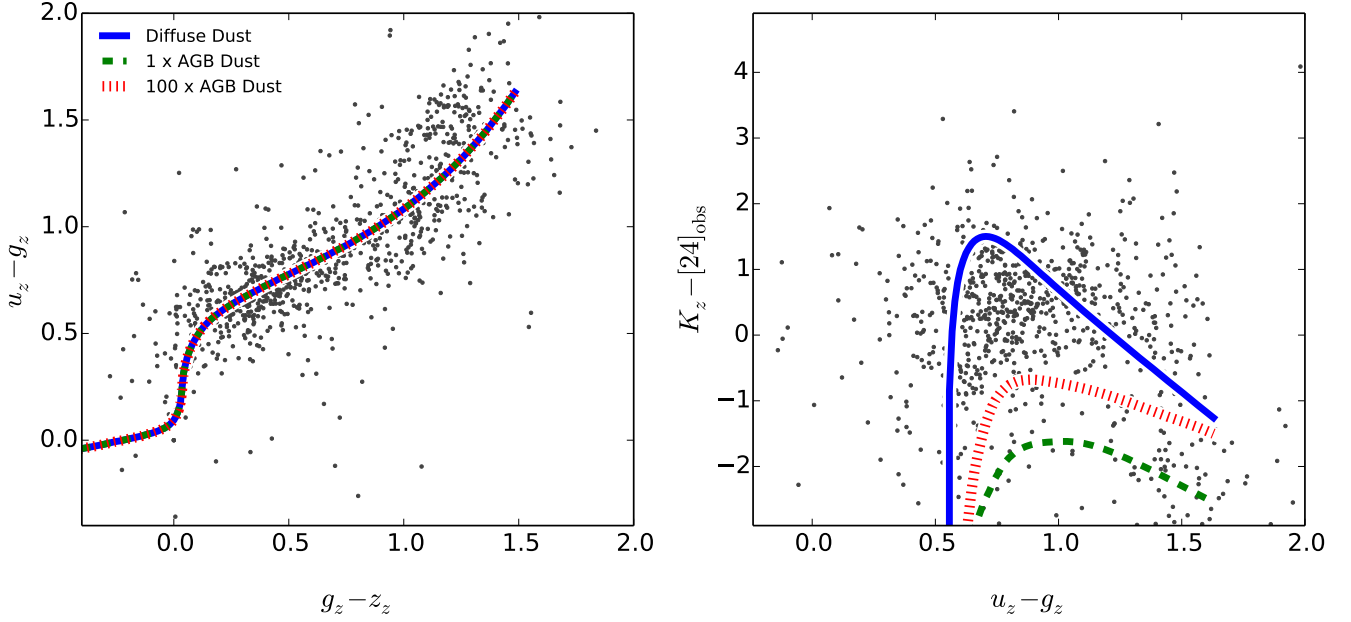


Figure 18. Color-color plots of galaxies at $z \sim 1$ from Wuyts et al. (2008). The data are compared to stellar population models with $\tau_{\text{SF}} = 2.0$ Gyr. Three models are plotted in each panel: a model with only diffuse dust (solid blue; $\tau_{\text{diff}} = 0.05$), a model with the default amount of AGB dust (dashed green), and a model with the AGB dust optical depth increased by a factor of 100 (red dotted). Along each line the model age varies from 10 Myr to 13 Gyr. The models without diffuse dust are unable to match the locus of mid-IR colors for the bulk of the galaxies (compare with Kelson & Holden 2010).

The luminosity functions proved to be a strong test of the AGB lifetimes in the Padova stellar models. The default Padova models produce too many stars even at $4.5\mu\text{m}$ where dust emission plays a minor role, suggesting that the circumstellar dust models are not the source of the discrepancy. After adjusting the lifetimes downward (by lowering their weight in the synthesis) we found good agreement for both the $4.5\mu\text{m}$ and $8.0\mu\text{m}$ LF for the LMC. However, the model SMC LF still substantially overpredicts the observed counts by factors of 3–5. Moreover, our recalibration of the Padova models produces relatively good agreement with AGB counts of low metallicity ANGST galaxies, with a typical overprediction of only 1.5 (in agreement with Girardi et al. 2010). This indicates that the Padova isochrones are doing well both at low metallicities probed by the ANGST galaxies ($Z < 0.15Z_{\odot}$) and LMC metallicity, but oddly not at SMC metallicity. The Girardi et al. (2010) dusty isochrones show a similar overprediction of the observed SMC luminosity function. This suggests that there is a problem with either the SMC IRAC LF, our adopted star formation history for the SMC, or perhaps there is some unknown issue with the models unique to SMC-like metallicities and ages.

There is a well-known degeneracy between stellar age and metallicity when modeling optical data that is typically only broken when the strengths of both balmer and metal lines can be accurately measured. Bressan et al. (1998) argued that circumstellar dust emission around AGB stars might also help to break this degeneracy, since the contribution of AGB stars to the bolometric luminosity varies strongly with time. We confirm the potential power of mid-IR emission as an age diagnostic by fitting ISO spectroscopy of NGC 1404, a galaxy with no on-going star formation. The models strongly prefer an

age of 7.5 Gyr and are capable of discriminating between even 1 – 2 Gyr differences in age at old times. Remarkably, the age derived in this way agrees very well with the analysis of the optical spectrum for this galaxy. The key limiting factor to deriving ages based on mid-IR data is systematic uncertainties in the modeling. Reducing these systematic uncertainties with targeted observations of AGB stars in the Local Group would enable firm absolute ages to be obtained in the mid-IR, even for old stellar populations.

With the IRAC and MIPS $24\mu\text{m}$ photometry and *Spitzer*-IRS spectroscopy presented by Martini et al. (2013) and Rampazzo et al. (2013), respectively, we constructed a small sample of quiescent, early-type galaxies lacking evidence for cold dust. The models presented here provide a reasonable fit to the data. This indicates that the majority of the mid-IR emission in these galaxies is dominated by circumstellar dust, as also argued by Martini et al. (2013). In detail, the models slightly over predict the $10\mu\text{m}$ silicate feature, which may be a reflection of our overly simplistic treatment of the grain species in the circumstellar shells.

Johnson et al. (2013) used CMD-based star formation histories to make predictions for the integrated light of nearby dwarf galaxies. Comparison of these predictions to observed total fluxes revealed good agreement in the FUV–NIR, but an offset was seen at $8\mu\text{m}$. We repeated this test with our updated models and found that the offset is reduced from 0.33 dex to 0.13 dex when circumstellar dust is included. We also compared the models to the observed $24\mu\text{m}$ flux and found that the offset without circumstellar dust, which is greater than a factor of 30, is only slightly reduced when circumstellar dust is included. It is likely that low levels of diffuse dust in these systems is providing the bulk of the observed $24\mu\text{m}$ emission.

There has been much discussion in the literature regarding the sources responsible for the mid-IR emission in typical star-forming galaxies. Possibilities include dust heated by young stellar populations, dust heated by old stellar populations, and circumstellar dust around AGB stars. Kelson & Holden (2010) suggested that the latter could play a large role in the mid-IR emission of star-forming galaxies. This possibility is not borne out in our models. Instead, circumstellar dust provides a rather small contribution to the mid-IR flux for galaxies with typical amounts of diffuse dust ($A_V \gtrsim 0.1$). This result does not preclude the possibility that evolved stars, including AGB stars, contribute substantially to the heating of the diffuse dust. Indeed, Salim et al. (2009) argued for this based on observations of star-forming galaxies at $z \sim 1$ (see also Utomo et al. 2014).

The launch of JWST will turn the spotlight on the $\sim 1 - 30\mu\text{m}$ SEDs of stellar populations across time. In this wavelength interval a variety of distinct physical processes contribute to the light, including PAH emission and circumstellar dust. Models such as the one presented in this paper will be necessary to interpret this data. In addition, JWST will provide stringent tests of these models by observing nearby AGB stars in detail and entire populations of such stars in nearby galaxies. In the process we hope to learn not only about the evolutionary history of galaxies but also about the physics shaping the final stages in the lives of AGB stars.

6. SUMMARY

We now summarize our main results.

- In agreement with previous work, our models indicate that the dusty circumstellar shells around AGB stars can have a factor of ~ 10 effect on the integrated flux of star clusters and galaxies at $\lambda \gtrsim 4\mu\text{m}$. The effect is especially large at intermediate ages $\sim 0.1 - 3$ Gyr and when the presence of diffuse dust is minimal. The emission associated with circumstellar dust shells may be important for interpreting the SEDs of quiescent galaxies at high redshift, where the average stellar age is relatively young.
- The presence of diffuse dust in a galaxy sharply reduces the influence of circumstellar dust emission at $\gtrsim 8\mu\text{m}$. At $24\mu\text{m}$, circumstellar dust contributes only $\sim 10\%$ of the flux for star-forming galaxies with $A_V \sim 0.1$. At shorter wavelengths (i.e., $< 10\mu\text{m}$), where under normal conditions diffuse dust does not contribute substantially, circumstellar dust may still play an important role.
- In early-type galaxies lacking signatures of cold diffuse dust, the mid-IR data is far in excess of a blackbody extrapolation at shorter wavelengths. Models that include circumstellar dust shells accurately reproduce the mid-IR photometry and spectra of early-type galaxies. The model MIR flux is sensitive to age, even at old ages. This suggests that this wavelength range can be a useful age diagnostic once circumstellar dust models have been accurately calibrated. The $10\mu\text{m}$ silicate feature is qualitatively well matched but there are some quantitative differences at the $\sim 10\%$ level.

We would like to thank Martha Boyer, Martin Groenewegen, Dan Kelson, Ivo Labbe, Sundar Srinivasan, Benjamin Sargent, and Roberto Rampazzo for generously sharing their data, and Paul Martini, Dan Kelson, and Julianne Dalcanton for fruitful conversations on this topic. We also thank the anonymous referee for their thoughtful comments that improved the quality of this manuscript. This project was supported in part by NASA grant NNX13AI46G.

REFERENCES

- Ahn, C. P., Alexandroff, R., Allende Prieto, C., et al. 2012, *ApJS*, 203, 21
- Aringer, B., Girardi, L., Nowotny, W., Marigo, P., & Lederer, M. T. 2009, *A&A*, 503, 913
- Athey, A., Bregman, J., Bregman, J., Temi, P., & Sauvage, M. 2002, *ApJ*, 571, 272
- Babbage, C. 1864, *Passages From the Life of a Philosopher* (London, Longman, Green, Longman, Roberts, Green,)
- Bedijn, P. J. 1987, *A&A*, 186, 136
- Beichman, C. A., Neugebauer, G., Habing, H. J., Clegg, P. E., & Chester, T. J., eds. 1988, *Infrared astronomical satellite (IRAS) catalogs and atlases. Volume 1: Explanatory supplement, Vol. 1*
- Berg, D. A., Skillman, E. D., Marble, A. R., et al. 2012, *ApJ*, 754, 98
- Blanco, A., Borghesi, A., Epifani, E., et al. 1998, *Ap&SS*, 262, 107
- Boyer, M. L., Srinivasan, S., van Loon, J. T., et al. 2011, *AJ*, 142, 103
- Bregman, J. N., Temi, P., & Bregman, J. D. 2006, *ApJ*, 647, 265
- Bressan, A., Granato, G. L., & Silva, L. 1998, *A&A*, 332, 135
- Cassarà, L. P., Piovan, L., Weiss, A., Salaris, M., & Chiosi, C. 2013, *MNRAS*, 436, 2824
- Charlot, S. & Fall, S. M. 2000, *ApJ*, 539, 718
- Chisari, N. E. & Kelson, D. D. 2012, *ApJ*, 753, 94
- Conroy, C. 2013, *ARA&A*, 51, 393
- Conroy, C., Graves, G. J., & van Dokkum, P. G. 2014, *ApJ*, 780, 33
- Conroy, C. & Gunn, J. E. 2010, *ApJ*, 712, 833
- Conroy, C., Gunn, J. E., & White, M. 2009, *ApJ*, 699, 486
- Dalcanton, J. J., Williams, B. F., Seth, A. C., et al. 2009, *ApJS*, 183, 67
- Dale, D. A., Cohen, S. A., Johnson, L. C., et al. 2009, *ApJ*, 703, 517
- Dell’Agli, F., Ventura, P., García Hernández, D. A., et al. 2014, *MNRAS*, 442, L38
- Di Criscienzo, M., Dell’Agli, F., Ventura, P., et al. 2013, *MNRAS*, 433, 313
- Draine, B. T. & Li, A. 2007, *ApJ*, 657, 810
- Ferrarotti, A. S. & Gail, H.-P. 2006, *A&A*, 447, 553
- Girardi, L., Marigo, P., Bressan, A., & Rosenfield, P. 2013, *ApJ*, 777, 142
- Girardi, L., Williams, B. F., Gilbert, K. M., et al. 2010, *ApJ*, 724, 1030
- González, R. A., Liu, M. C., & Bruzual A., G. 2004, *ApJ*, 611, 270
- González-Lópezlira, R. A., Bruzual-A., G., Charlot, S., Ballesteros-Paredes, J., & Loinard, L. 2010, *MNRAS*, 403, 1213
- Gordon, K. D., Meixner, M., Meade, M. R., et al. 2011, *AJ*, 142, 102
- Groenewegen, M. A. T. 2006, *A&A*, 448, 181
- Groenewegen, M. A. T., Barlow, M. J., Blommaert, J. A. D. L., et al. 2012, *A&A*, 543, L8
- Groenewegen, M. A. T., Sloan, G. C., Soszyński, I., & Petersen, E. A. 2009, *A&A*, 506, 1277
- Groenewegen, M. A. T., Waelkens, C., Barlow, M. J., et al. 2011, *A&A*, 526, A162
- Habing, H. J., Tignon, J., & Tielens, A. G. G. M. 1994, *A&A*, 286, 523
- Harris, J. & Zaritsky, D. 2004, *AJ*, 127, 1531
- . 2009, *AJ*, 138, 1243
- Iben, Jr., I. & Renzini, A. 1983, *ARA&A*, 21, 271
- Ita, Y., Onaka, T., Kato, D., et al. 2008, *PASJ*, 60, 435
- Ivezic, Z. & Elitzur, M. 1997, *MNRAS*, 287, 799

- Ivezic, Z., Nenkova, M., & Elitzur, M. 1999, DUSTY: Radiation transport in a dusty environment, astrophysics Source Code Library
- Jimenez, R., Bernardi, M., Haiman, Z., Panter, B., & Heavens, A. F. 2007, *ApJ*, 669, 947
- Johnson, B. D., Weisz, D. R., Dalcanton, J. J., et al. 2013, *ApJ*, 772, 8
- Jones, O. C., Kemper, F., Sargent, B. A., et al. 2012, *MNRAS*, 427, 3209
- Jura, M., Kim, D. W., Knapp, G. R., & Guhathakurta, P. 1987, *ApJ*, 312, L11
- Kelson, D. D. & Holden, B. P. 2010, *ApJ*, 713, L28
- Kemper, F., Woods, P. M., Antoniou, V., et al. 2010, *PASP*, 122, 683
- Kennicutt, R. C. & Evans, N. J. 2012, *ARA&A*, 50, 531
- Knapp, G. R., Guhathakurta, P., Kim, D.-W., & Jura, M. A. 1989, *ApJS*, 70, 329
- Kriek, M., Labbé, I., Conroy, C., et al. 2010, *ApJ*, 722, L64
- Larson, R. B. & Tinsley, B. M. 1978, *ApJ*, 219, 46
- Lauer, T. R., Faber, S. M., Gebhardt, K., et al. 2005, *AJ*, 129, 2138
- Le Bertre, T. 1987, *A&A*, 176, 107
- . 1992, *A&AS*, 94, 377
- Lee, H., Skillman, E. D., Cannon, J. M., et al. 2006, *ApJ*, 647, 970
- Lejeune, T., Cuisinier, F., & Buser, R. 1997, *A&AS*, 125, 229
- Maraston, C. 2005, *MNRAS*, 362, 799
- Marigo, P., Bressan, A., Nanni, A., Girardi, L., & Pumo, M. L. 2013, *MNRAS*, 434, 488
- Marigo, P., Girardi, L., Bressan, A., et al. 2008, *A&A*, 482, 883
- Martini, P., Dicken, D., & Storch-Bergmann, T. 2013, *ApJ*, 766, 121
- McDonald, I., Sloan, G. C., Zijlstra, A. A., et al. 2010, *ApJ*, 717, L92
- Meixner, M., Gordon, K. D., Indebetouw, R., et al. 2006, *AJ*, 132, 2268
- Melbourne, J. & Boyer, M. L. 2013, *ApJ*, 764, 30
- Melbourne, J., Williams, B. F., Dalcanton, J. J., et al. 2012, *ApJ*, 748, 47
- Nanni, A., Bressan, A., Marigo, P., & Girardi, L. 2013, *MNRAS*, 434, 2390
- Noël, N. E. D., Conn, B. C., Carrera, R., et al. 2013, *ApJ*, 768, 109
- Pessev, P. M., Goudfrooij, P., Puzia, T. H., & Chandar, R. 2008, *MNRAS*, 385, 1535
- Piovan, L., Tantalò, R., & Chiosi, C. 2003, *A&A*, 408, 559
- Rampazzo, R., Panuzzo, P., Vega, O., et al. 2013, *MNRAS*, 432, 374
- Rosenfield, P., Marigo, P., Girardi, L., et al. 2014, *ApJ*, 790, 22
- Salim, S., Dickinson, M., Michael Rich, R., et al. 2009, *ApJ*, 700, 161
- Sargent, B. A., Srinivasan, S., & Meixner, M. 2011, *ApJ*, 728, 93
- Sargent, B. A., Srinivasan, S., Meixner, M., et al. 2010, *ApJ*, 716, 878
- Schneider, R., Valiante, R., Ventura, P., et al. 2014, *MNRAS*, 442, 1440
- Searle, L., Sargent, W. L. W., & Bagnuolo, W. G. 1973, *ApJ*, 179, 427
- Silva, L., Granato, G. L., Bressan, A., & Danese, L. 1998, *ApJ*, 509, 103
- Skrutskie, M. F., Cutri, R. M., Stiening, R., et al. 2006, *AJ*, 131, 1163
- Srinivasan, S., Sargent, B. A., Matsuura, M., et al. 2010, *A&A*, 524, A49
- Srinivasan, S., Sargent, B. A., & Meixner, M. 2011, *A&A*, 532, A54
- Suh, K.-W. 1999, *MNRAS*, 304, 389
- . 2000, *MNRAS*, 315, 740
- . 2002, *MNRAS*, 332, 513
- Tem, P., Brighenti, F., & Mathews, W. G. 2009, *ApJ*, 707, 890
- Thomas, D., Maraston, C., Bender, R., & Mendes de Oliveira, C. 2005, *ApJ*, 621, 673
- Tinsley, B. M. 1972, *A&A*, 20, 383
- Trager, S. C., Worthey, G., Faber, S. M., Burstein, D., & González, J. J. 1998, *ApJS*, 116, 1
- Trager, S. C., Worthey, G., Faber, S. M., & Dressler, A. 2005, *MNRAS*, 362, 2
- Utomo, D., Kriek, M., Labbé, I., Conroy, C., & Fumagalli, M. 2014, *ApJ*, 783, L30
- Vassiliadis, E. & Wood, P. R. 1993, *ApJ*, 413, 641
- Ventura, P., Dell'Agli, F., Schneider, R., et al. 2014, *MNRAS*, 439, 977
- Walcher, J., Groves, B., Budavári, T., & Dale, D. 2011, *Ap&SS*, 331, 1
- Weisz, D. R., Dalcanton, J. J., Williams, B. F., et al. 2011, *ApJ*, 739, 5
- Wuyts, S., Labbé, I., Schreiber, N. M. F., et al. 2008, *ApJ*, 689, 653
- Zaritsky, D., Harris, J., & Thompson, I. 1997, *AJ*, 114, 1002
- Zibetti, S., Gallazzi, A., Charlot, S., Pasquali, A., & Pierini, D. 2012, in *IAU Symposium*, Vol. 284, IAU Symposium, ed. R. J. Tuffs & C. C. Popescu, 63–65